สำนักหอสมุดกลาง พระจอมเกล้าลาดกระบัง

POSITION CONTROL OF ULTRASONIC LINEAR MOTOR USING PDFF CONTROLLER DESIGNED BY CDM

DON ISARAKORN

King Mongkut's Institute of Technology Ladkrabang

A THESIS SUBMITTED IN PARTIAL FULFILLMENT

OF THE REQUIREMENTS FOR THE DEGREE OF

MASTER OF ENGINEERING IN CONTROL ENGINEERING

SCHOOL OF GRADUATE STUDIES

KING MONGKUT'S INSTITUTE OF TECHNOLOGY LADKRABANG

2003

ISBN 974-324-602-9

เลขหมู่.....
เลขทะเบียน.....41535
วัน, เดือน, ปี.....30 มี.ค. 2547

.b.....
.i.....

This material is reserved for educational use only, not allowed for commercial use.
Prohibited to modify content, and cite the document when use.

COPYRIGHT 2003

SCHOOL OF GRADUATE STUDIES

KING MONGKUT'S INSTITUTE OF TECHNOLOGY LADKRABANG

This material is reserved for educational use only, not allowed for commercial use.

Forbidden to modify the content, and cite the document when use.

หัวข้อวิทยานิพนธ์	การควบคุมตำแหน่งของอัลตร้าโซนิคลิเนียร์มอเตอร์โดยใช้ตัวควบคุมพีดีเอฟเอฟที่ออกแบบด้วยวิธีแผนผังค่าสัมประสิทธิ์
นักศึกษา	นายดอน อิศรากร
รหัสนักศึกษา	44061506
ปริญญา	วิศวกรรมศาสตรมหาบัณฑิต
สาขาวิชา	วิศวกรรมระบบควบคุม
พ.ศ.	2546
อาจารย์ผู้ควบคุมวิทยานิพนธ์	รศ.ดร.จงกล งามวิวิทย์

บทคัดย่อ

อัลตร้าโซนิคลิเนียร์มอเตอร์เป็นมอเตอร์ที่มีคุณสมบัติดีหลายประการเช่น ความเร็วต่ำ ขนาดเล็ก น้ำหนักเบา แรงผลักสูง ไม่มีการแผ่สนามแม่เหล็กไฟฟ้า ด้วยเหตุนี้จึงได้มีการพัฒนามอเตอร์ชนิดนี้ให้มีโครงสร้างทางกายภาพที่แตกต่างกันเพื่อนำมาใช้เป็นตัวขับเร้าในระบบควบคุมการเคลื่อนที่ แต่ระบบควบคุมการเคลื่อนที่ของอัลตร้าโซนิคลิเนียร์มอเตอร์ที่ถูกนำเสนอในบทความวิจัยที่ผ่านมาพบว่า มีหลักการที่ค่อนข้างซับซ้อนและยุ่งยากต่อการนำไปสร้างใช้งานจริง เช่น การควบคุมโดยใช้กฎฟัซซี การควบคุมโดยใช้โครงข่ายประสาท การควบคุมแบบปรับตัวได้ เป็นต้น ดังนั้น วิทยานิพนธ์ฉบับนี้จึงนำเสนอหลักการควบคุมตำแหน่งของอัลตร้าโซนิคลิเนียร์มอเตอร์โดยใช้ตัวควบคุมพีดีเอฟเอฟที่ออกแบบด้วยวิธีแผนผังค่าสัมประสิทธิ์ ซึ่งเป็นวิธีที่ง่ายและมีประสิทธิภาพในการออกแบบพารามิเตอร์ของตัวควบคุม จากผลการจำลองและการทดลองแสดงให้เห็นถึงสมรรถนะของระบบควบคุมที่นำเสนอ

This material is reserved for educational use only, not allowed for commercial use.
Forbidden to modify the content, and cite the document when use.

Thesis Title	Position Control of Ultrasonic Linear Motor using PDFF Controller Designed by CDM
Student	Mr. Don Isarakorn
Student ID.	44061506
Degree	Master of Engineering
Programme	Control Engineering
Year	2003
Thesis Advisor	Assoc.Prof. Dr. Jongkol Ngamwiwit

ABSTRACT

An ultrasonic linear motor has many excellent performances such as high precision, quick response, hard break with no backlash, high power to weight ratio and negligible EMI. A variety of ultrasonic linear motors have been developed and used as an actuator in motion control systems. In recent years, a number of control schemes have been proposed to control the position of ultrasonic linear motors, such as fuzzy reasoning control, neural network and adaptive control. However, these control schemes are complex and hard to apply to actual implementation. Hence, this thesis presents a new position control scheme for ultrasonic linear motor using a pseudo-derivative control with feedforward gains (PDFF) controller designed by the coefficient diagram method (CDM) which is an efficient and simple method to design the parameters of PDFF controller. The effectiveness of the proposed control scheme is demonstrated by the several simulations and experiments.

This material is reserved for educational use only, not allowed for commercial use.
Forbidden to modify the content, and cite the document when use.

ACKNOWLEDGMENTS

I would like to thank my advisor, Dr. Jongkol Ngamwiwit, for her support and guidance during the course of this research work. Without her suggestions, I would have never accomplished this work.

Thanks to Ajarn Taworn Benjanarasuth and all the members of the Control and Mechatronics Lab for the excellent support and advice throughout the year.

This thesis would not have been possible without JICA for supporting on research tools. I also wish to thank the Ministry of University Affairs for the financial support.

Finally, I would like to express my boundless gratitude to my beloved parents for their loves and taking care of me.

King Mongkut's Institute of Technology Ladkrabang

This material is reserved for educational use only, not allowed for commercial use.
Forbidden to modify the content, and cite the document when use.

CONTENTS

This material is reserved for educational use only, not allowed for commercial use.

Forbidden to modify the content, and cite the document when use.

CONTENTS (Cont.)

This material is reserved for educational use only, not allowed for commercial use.
Forbidden to modify the content, and cite the document when use.

LIST OF TABLES

This material is reserved for educational use only, not allowed for commercial use.
Forbidden to modify the content, and cite the document when use.

LIST OF FIGURES

This material is reserved for educational use only, not allowed for commercial use.

Forbidden to modify the content, and cite the document when use.

LIST OF FIGURES (Cont.)

This material is reserved for educational use only, not allowed for commercial use.

Forbidden to modify the content, and cite the document when use.

LIST OF FIGURES (Cont.)

This material is reserved for educational use only, not allowed for commercial use.
Forbidden to modify the content, and cite the document when use.

NOMENCLATURE

A	Force factor
$A_c(s)$	Denominator polynomial of controller
$A_p(s)$	Denominator polynomial of plant
$A_p^*(s)$	Denominator polynomial of plant included the feedback controller
b	Viscous damping coefficient
$B_a(s)$	Pre-filter
$B_c(s)$	Numerator polynomial of controller
$B_{fb}(s)$	Polynomial of feedback controller
$B_{ff}(s)$	Polynomial of feedforward controller
$B_p(s)$	Numerator polynomial of plant
$B_p^*(s)$	Numerator polynomial of plant included the feedback controller
C_d	Blocking capacitance
C_m	Equivalent capacitance
$C(s)$	Output
D	Electric flux density
$D(s)$	Disturbance
E	Electric field
F	Force
F_n	Normal force
f_s	Driving frequency
F_t	Thrust force
$G_p(s)$	Plant
$G_p^*(s)$	Modified plant
k	Wave number
K	Spring constant
K_d	Derivative gain of feedback controller
K_{df}	Derivative gain of feedforward controller
k_f	Thrust force constant
K_i	Integral gain

This material is reserved for educational use only, not allowed for commercial use.
Forbidden to modify the content, and cite the document when use.

NOMENCLATURE (Cont.)

K_p	Proportional gain of feedback controller
K_{pf}	Proportional gain of feedforward controller
L_m	Equivalent inductance
m	Mass of piezoelectric-ceramic-metal element
M	Slider mass
$P(s)$	Characteristic polynomial
r_d	Dielectric-loss resistance
r_o	Internal resistance
$R(s)$	Input
$U(s)$	Control signal
$u_s(x,t)$	Wave function of standing wave
$u_t(x,t)$	Wave function of traveling wave
v	Velocity
V_c	Constant control input voltage
V_{in}	Control input voltage
ω_o	Resonant frequency
ω_r	Antiresonant frequency
x	Distance
x_{ss}	Steady-state response
Y_d	Blocking admittance
Z_m	Internal impedance
θ	Angle
α	Tuning factor
ω	Angular frequency
ζ	Damping ratio
γ_i	Stability index
γ_i^*	Stability limit
τ	Equivalent time constant

This material is reserved for educational use only, not allowed for commercial use.
Forbidden to modify the content, and cite the document when use.

Chapter 1

Introduction

1.1 Statement and Significance of the Problems

An ultrasonic linear motor is a type of actuator that uses mechanical vibrations in the ultrasonic range as its drive source [1]. The ultrasonic linear motor operates on an indirect-drive principle which uses piezoelectric ceramic elements to generate ultrasonic waves and produce a linear motion. The characteristics of ultrasonic linear motor are high resolution, unlimited travel, wide dynamic range of velocity, hold stability at power off and a small compact size. While the ultrasonic linear motor has high potential for application in precision position control system, the highly nonlinear features associated with the dynamics of these elements are challenges to how efficiently these potentials can be realized [2].

In recent years, many control schemes have been proposed to control the position of ultrasonic motors, such as fuzzy reasoning control [3-5], neural network [6-7] and adaptive control [8-12]. Fuzzy reasoning control is a simple technique to control a complex system because it does not need to use a mathematical model. Nevertheless, extract of fuzzy rules depends on experience and intuition of the designer, and its tuning is tedious duties. Adaptive control algorithm has been used to maintain good performance of the servo system subjected to torque disturbance and parameter variations. However, adaptive control techniques have many difficulties when applying to actual implementation. Neural network has a good potential for control applications because it can approximate the nonlinear input-output mappings of the plant, but there is some error while the network is learning.

Hence, this thesis proposes a new position control scheme for ultrasonic linear motor using a pseudo-derivative control with feedforward gains (PDFF) controller designed by the coefficient diagram method (CDM) [13]. The PDFF control system compromises both tracking and disturbance rejection performances [14]. The CDM is an efficient tool to design the parameters of PDFF controller to meet the three major characteristics of control system, namely system stability, response speed and robustness.

This material is reserved for educational use only, not allowed for commercial use.
Forbidden to modify the content, and cite the document when use.

1.2 Research Objective and Approach Methodology

The need to control the position of ultrasonic linear motor with high performance has motivated the following studies:

1) The electrical-to-mechanical energy transformation of piezoelectric material and its mathematical equations as well as basic wave equation are studied. These are the fundamental concepts to understand the action of each component of an ultrasonic linear motor, and lead to drive it efficiently.

2) Derivation of ultrasonic linear motor model. In this work, the ultrasonic linear motor is modeled to be a linear system in order that CDM can be applied. The model parameters are determined from experimental data.

3) Study of the PDFF controller for position control system. The PDFF controller can be designed to satisfy both the tracking and regulation performances, which are the most important for the precision position control system. However, it is quite complicated to design the PDFF controller parameters because this controller requires tuning of the additional parameters [15]. Hence, the CDM is adopted to design the PDFF controller parameters. The parameters are obtained properly and easily.

4) Designing method for controller is proposed. The feedforward and feedback controllers are added to the CDM standard block diagram of SISO system [16]. The plant and the controllers are represented in polynomial form. The stability index γ_i and the equivalent time constant τ are defined based on the CDM while the tuning factor α is defined as $0 < \alpha \leq 1$. The coefficients of numerator and denominator polynomials of the closed-loop transfer function obtained from the proper γ_i, τ and α are related to the PDFF controller parameters.

5) Implementation of PDFF controller for the ultrasonic linear motor. The effectiveness of PDFF control algorithm used to control the position of ultrasonic linear motor is shown in three aspects: response of position control system, disturbance rejection capability and position tracking characteristic.

This material is reserved for educational use only, not allowed for commercial use.
Forbidden to modify the content, and cite the document when use.

1.3 Summary of Thesis Contents

This thesis is organized in 6 chapters including references and appendices.

Chapter 2 describes the fundamentals of ultrasonic linear motor, such as operating principle, motor classification, modeling and etc.

Chapter 3 explains the basics of the CDM, which consist of the CDM standard block diagram, basic mathematical relations concerning with the CDM and coefficient diagram.

Chapter 4 introduces the structure of PDFF controller and propose a general form of PDFF control system for designing controller parameters by CDM. In this chapter, the overview of the PDFF controller will be made first, and then the control system structure will be presented. Finally, the design procedure will be explained.

Chapter 5 presents the application of PDFF controller to control the position of ultrasonic linear motor. The experimental equipments will be described first. Then, the model of ultrasonic linear motor will be found from experimental data. Finally, several simulation and experimental results will be performed.

Chapter 6 concludes the results of this research and future works.

King Mongkut's Institute of Technology Ladkrabang

This material is reserved for educational use only, not allowed for commercial use.
Forbidden to modify the content, and cite the document when use.

Chapter 2

Introduction to Ultrasonic Linear Motor

The ultrasonic linear motor is an innovative manipulator that has shown a high potential in application that the manipulation within the micrometer is required. This motor uses mechanical vibrations in the ultrasonic range to generate the thrust force in stead of electromagnetic field. The use of ultrasonic waves is a direct outcome of using piezoelectric ceramic elements, which expand or contract in accordance with an applied electric field, as the vibrational source. In the ultrasonic linear motor, a sinusoidal voltage is applied to the piezoelectric ceramic elements to generate alternating expansions and contractions in the ceramic body itself. The oscillations are mechanically rectified in the motor to obtain the linear motion. The ultrasonic linear motor has now been investigated for several years. Their key features are high trust forces related to volume and good position-accuracy. A variety of ultrasonic linear motors have been developed and used as an actuator in motion control systems.

2.1 Operating Principle of Ultrasonic Linear Motor

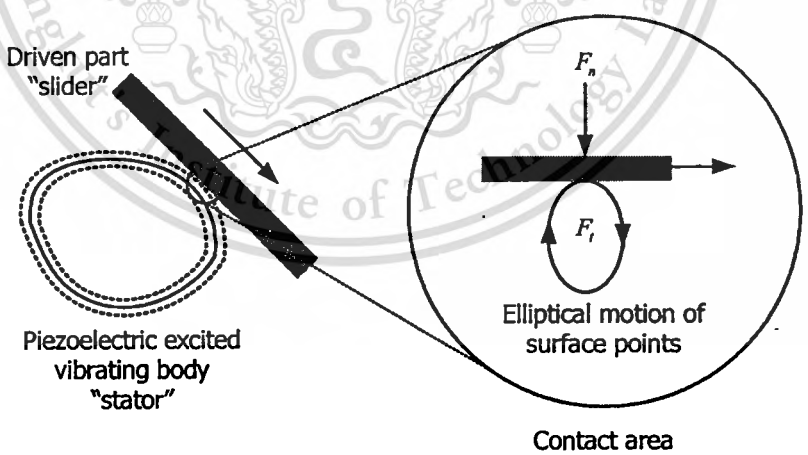

Figure 2.1 Operating principle of ultrasonic linear motor.

The operating principle is based on piezoelectric ceramic elements that convert electrical energy to mechanical energy in the form of vibrations. Most often the piezoelectric ceramic elements are attached to an elastic body (stator), which are excited by the inverse piezoelectric effect. The points of its surface then perform elliptical motions with a frequency in the ultrasonic

Forbidden to modify the content, and cite the document when use.

range. Another body (slider) is pressed against the elastic body by a static normal force F_n, and thus each vibration cycle is transformed to continuous motion by friction forces F_t. A picture depicting this operation is shown in figure 2.1.

Based on this operating principle, many different types of ultrasonic linear motors have been developed. The merits and demerits of ultrasonic linear motor are summarized in Table 2.1.

Table 2.1 Merits and demerits of ultrasonic linear motors

Merits	Demerits
• Low Speed and High Torque	• High Frequency Power Supply Required
• Direct Drive	• Highly Nonlinear Features
• Quick Response	• Low Durability
• Wide Range of Speeds	
• Hard Break with No Backlash	
• Excellent Controllability	
• Fine Position Resolution	
• High Power-to-Weight Ratio	
• Quiet Drive	
• Compact Size and Light Weight	
• Simple Structure	
• No Generation of Electromagnetic Radiation	
• Unaffected by External Electric or Magnetic Fields	

2.2 Classification of Ultrasonic Linear Motors

There are many different types of mechanical structures to achieve the desired elliptical motion of surface points. The main distinctive feature for classifying ultrasonic linear motors is the utilized vibration type. The vibration induced in the motor is either in the form of a standing wave or a traveling wave. The standing wave is described by

This material is reserved for educational use only, not allowed for commercial use.
Forbidden to modify the content, and cite the document when use.

$$u_s(x,t) = A\ \cos(kx)\ \ \cos(\omega t)\ , \tag{2.1}$$

while the equation for a traveling wave is

$$u_t(x,t) = A\cos(kx - \omega t), \tag{2.2}$$

where $u_s(x,t)$ and $u_t(x,t)$ denote the wave functions of standing wave and traveling wave respectively, and k is wave number. Equation (2.2) can be rewritten as

$$u_t(x,t) = A\ \cos(kx)\ \ \cos(\omega t)\ + A\ \cos(kx - \pi/2)\ \ \cos(\omega t - \pi/2)\ . \tag{2.3}$$

This equation shows that a traveling wave can be generated by superposing two standing waves with a phase difference of 90 degrees between them. This is the only feasible way to generate a stable traveling wave in a structure of finite size and volume.

2.2.1 Standing Wave Motor

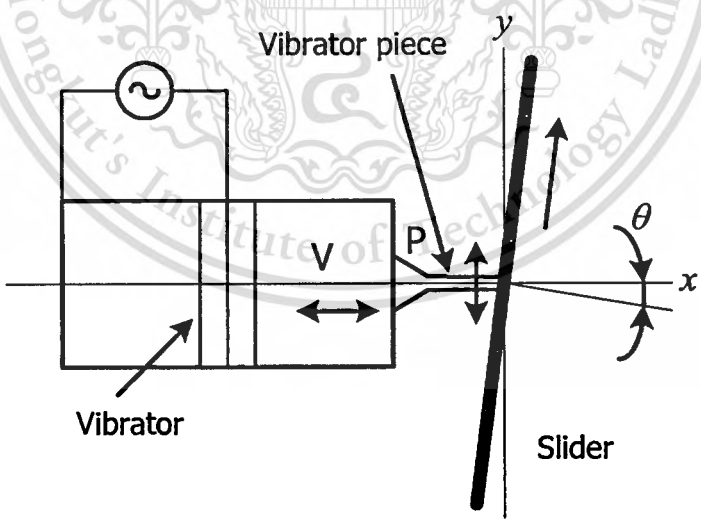

Figure 2.2 Basic structure of standing wave motor.

The standing wave motor is sometimes referred to a vibratory coupler motor. A vibratory piece P is connected to the vibrator V and the tip portion executes an elliptical displacement as shown in figure 2.2 The motion of the tip of the vibrator piece P while vibrator V is being driven will be examined, taking the x-axis in the longitudinal direction and the y-axis normal to the x-

This material is reserved for educational use only, not allowed for commercial use.
Forbidden to modify the content, and cite the document when use.

axis. When the vibrator V is oscillating, the base of the vibratory piece P moves in the horizontal direction. At the tip, however, vertical movement is caused by the thrust force F_t, which is the tangential component of the force of piece produced owing to the angle of slant θ. Combining the synchronous harmonic motions in both directions, the tip will follow an elliptical path.

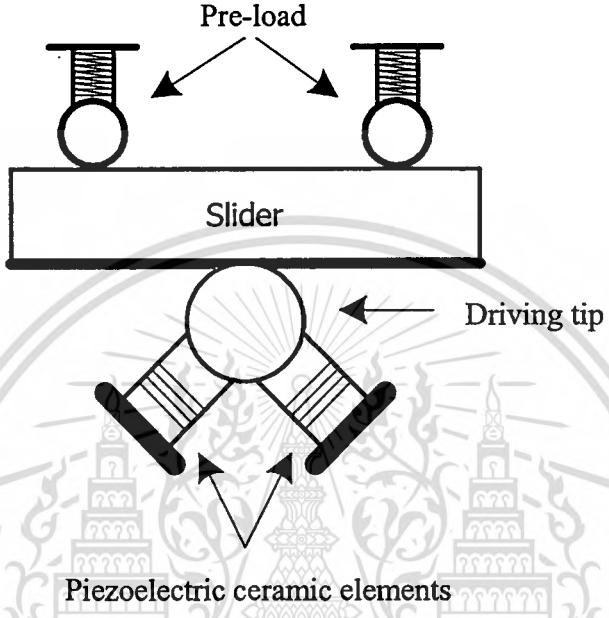

Figure 2.3 Structure of standing wave motor driven by two piezoelectric ceramic elements.

The standing wave motor has the advantages of low production cost, simple structure and high efficiency. The fundamental disadvantages of this design are related to some variability of the locus, and the motion in both clockwise and counterclockwise directions is generally not well controlled due to require only a single vibration source. In order to achieve the reversible movement, double vibration sources are required. Figure 2.3 shows, for instance, the structure of standing wave motor driven by two vibration sources. The two piezoelectric ceramic elements are positioned orthogonal to each other in order to generate the elliptical motion of the tip, and control the direction of the slider.

2.2.2 Traveling Wave Motor

The superposition of two standing waves with a 90-degree phase difference produces a traveling wave. A particle on the surface of the elastic body (stator) executes a displacement with an elliptical locus due to the coupling of longitudinal and transverse waves as shown in figure 2.4. This motor requires two vibrational sources to generate the traveling wave, leading to a rather low

Forbidden to modify the content, and cite the document when use.

efficiency. The moving direction is readily changed by switching the phase difference from 90 to –90 degrees.

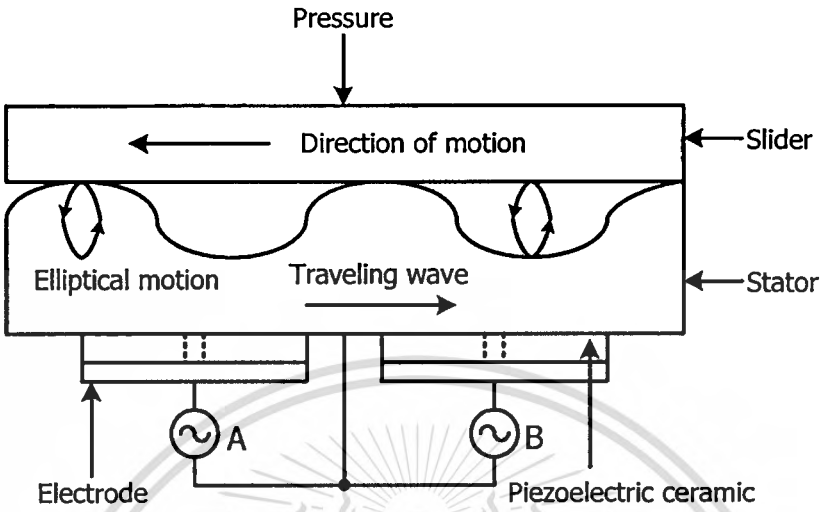

Figure 2.4 Principle of traveling wave motor.

An ultrasonic linear motor driven by two bending vibrations is shown in figure 2.5. The two piezoelectric vibrators installed at both ends of a transmittance steel rod. A piezoelectric vibrator acts as a vibrator and produce the traveling wave to the other one that acts as an absorber. Adjustment of the load resistance Z of the absorber produces a perfect traveling wave. Movement in the reverse direction is induced by exchanging the exciting and receiving roles of the piezoelectric vibrators.

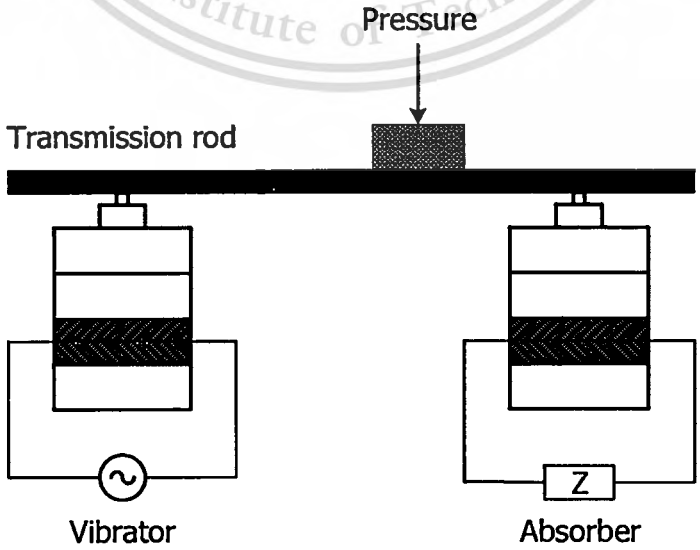

Figure 2.5 Linear motor driven by two bending vibrations.

This material is reserved for educational use only, not allowed for commercial use.
Forbidden to modify the content, and cite the document when use.

2.3 Ultrasonic Linear Motor Drive/Control Techniques

Piezoelectric ceramics play a vital role in the ultrasonic linear motor because they serve as vibrational sources of the motor. The conversion of electrical energy into mechanical oscillations takes place in the piezoelectric ceramics. To understand how to drive the ultrasonic linear motor, a basic equivalent circuit of piezoelectric ceramic must be regarded. Consider the basic equivalent circuit of piezoelectric ceramic shown in figure 2.6 (detail in Appendix A).

The elements in this equivalent circuit have the following meanings:

C_d : blocking capacitor (acts as a regular dielectric)

L_m : equivalent inductor (represents the mass effect of the ceramic body and driving tip)

C_m : equivalent capacitor (represents the spring effect of the ceramic body and driving tip)

r_o : resistance representing losses that occur within the ceramic body and driving tip.

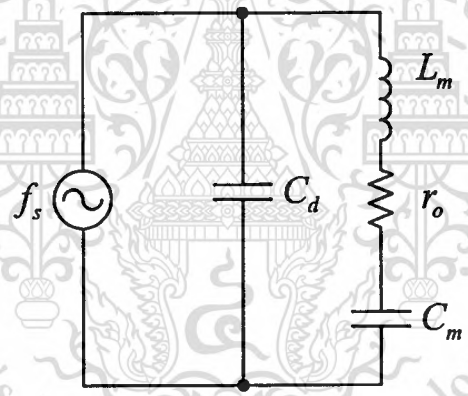

Figure 2.6 Basic equivalent circuit of piezoelectric ceramic.

When an alternating electric field is applied to the piezoelectric ceramic, the mechanical vibration is excited. If the driving frequency f_s is adjusted to the mechanical resonance frequency ω_o of the device, a large resonant strain is generated. This phenomenon is called "piezoelectric resonance" and is very useful for applications such as actuators. At the resonant frequency ω_o, the impedance of the equivalent circuit in figure 2.6 has a minimum value. Conversely, there is a frequency at which the impedance has a maximum value. This is called the antiresonant frequency ω_r (see figure 2.7). Thus, from figure 2.6, the response of the ultrasonic linear motor is not directly proportional to the magnitude of applied voltage, but is dependent of the driving frequency f_s. The ultrasonic linear motor has a maximum speed when the driving

This material is reserved for educational use only, not allowed for commercial use.
Forbidden to modify the content, and cite the document when use.

frequency f_s closes to the resonant frequency ω_o. In addition, the speed can be adjusted by changing the driving frequency f_s. This technique is called the "resonance drive", which is widely used for piezoelectric actuators. Moreover, there are the other methods for controlling the ultrasonic linear motor, such as phase drive [7], voltage drive [17] and pulse width modulation [18].

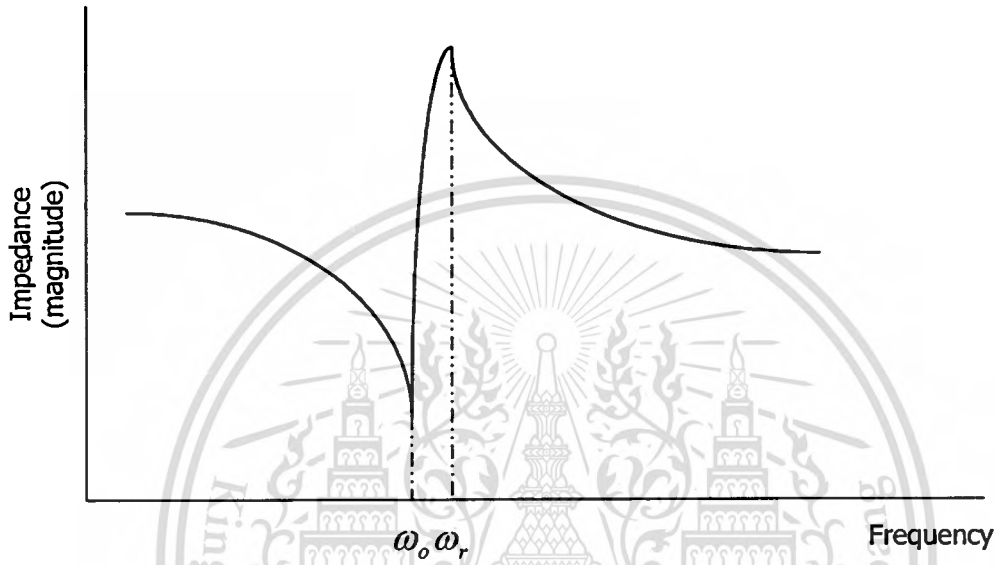

Figure 2.7 Resonant frequency ω_o and antiresonant frequency ω_r.

2.4 Modeling of Ultrasonic Linear Motor

The friction force acts as the driving force of the ultrasonic linear motor. Thus, it is not easy to find an explicit mathematical friction model for the ultrasonic linear motor because friction plays a dual role. It provides the primary transfer mechanism to bring about the motion, while it opposes the realization of precision motion control. For the methodology of controller designed by CDM, the model of ultrasonic linear motor must be known roughly and be linearized. In following sub-section, how to model the ultrasonic linear motor to be a linear system will be described.

2.4.1 Mathematical Model

The structure of ultrasonic linear motor is shown in figure 2.8. The ultrasonic linear motor is driven through the inverter. An AC voltage converted from DC source voltage by the converter is fed to the motor with the proper frequency. This frequency, however, can be adjusted by the control input voltage V_{in}, which represents the thrust force F_t (N) generated from piezoelectric

Forbidden to modify the content, and cite the document when use.

ceramic and transmitted to the driving tip. Therefore, the relation between the control input voltage V_{in} and the thrust force F_t can be expressed by

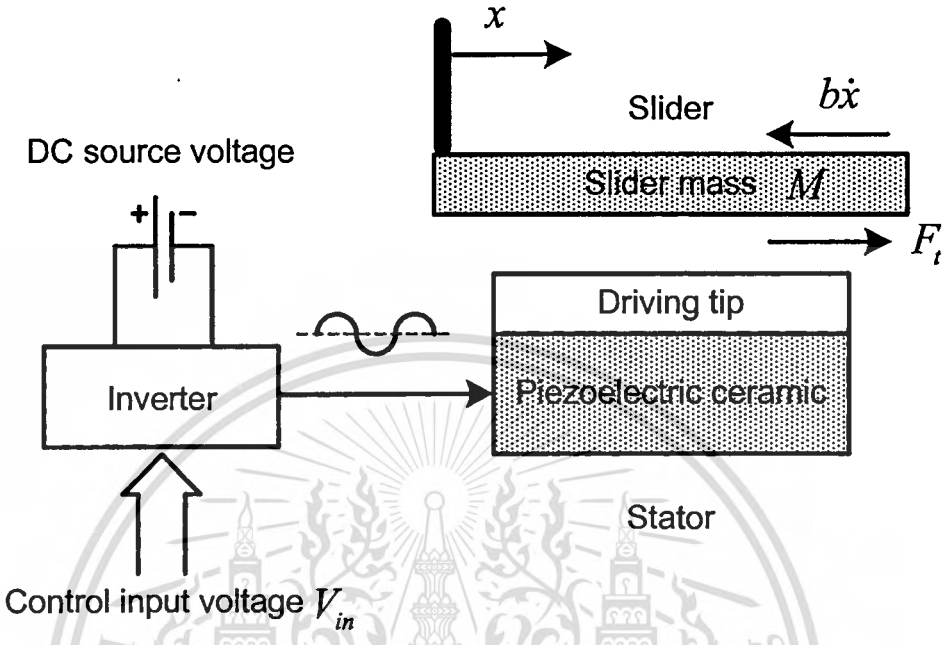

Figure 2.8 Structure of ultrasonic linear motor.

$$F_t = k_f V_{in}, \tag{2.4}$$

where k_f denotes the thrust force constant (N/V). The thrust force F_t serves as the driving force for the slider. By the Newton's second law, the equation of motion for the slider is

$$M\ddot{x} = F_t - b\dot{x} \tag{2.5}$$

where M represents the slider mass (kg), x is the position (m), and b is the viscous damping coefficient ($N.\text{sec}/m$).

Static and coulomb frictions would also be presented to some degree, but they must be neglected in a linearized analysis. Substituting F_t of equation (2.4) into equation (2.5) and rearranging, we get

$$M\ddot{x} + b\dot{x} = k_f V_{in}. \tag{2.6}$$

This material is reserved for educational use only, not allowed for commercial use.
Forbidden to modify the content, and cite the document when use.

Taking the Laplace transform of this equation, assuming zero initial conditions, we obtain

$$\left[Ms^2 + bs\right]X(s) = k_f V_{in}(s). \tag{2.7}$$

Hence, the ultrasonic linear motor transfer function from the control input voltage $V_{in}(s)$ to the position $X(s)$ is

$$G_p(s) = \frac{X(s)}{V_{in}(s)} = \frac{k_f}{s(Ms+b)}. \tag{2.8}$$

The model is second-order system and the system type is one.

2.4.2 Parameter Identification

By applying the control input voltage V_{in} to the system of figure 2.8, the output of the system can be obtained as

$$X(s) = \frac{k_f}{s(Ms+b)}\frac{V_c}{s}, \tag{2.9}$$

where V_c is the magnitude of the constant control input. Expanding $X(s)$ into partial fractions gives

$$X(s) = \frac{k_f V_c}{b}\left[\frac{1}{s^2} - T\frac{1}{s} + \frac{T^2}{Ts+1}\right], \tag{2.10}$$

where

$$T = \frac{M}{b}. \tag{2.11}$$

Taking the inverse Laplace transform of equation (2.10), we obtain

$$x(t) = \frac{k_f V_c}{b}\left[t - T + Te^{-t/T}\right], \quad \text{for } t \geq 0 \tag{2.12}$$

This material is for educational use only. Not allowed for commercial
Forbidden to modify the content, and cite the document when use.

The response curve of equation (2.12) to the constant control input voltage V_c is shown in figure 2.9. As t approaches infinity, the equation for the steady-state response x_{ss} can be written by

$$x_{ss} = \frac{k_f V_c}{b}(t - T). \tag{2.13}$$

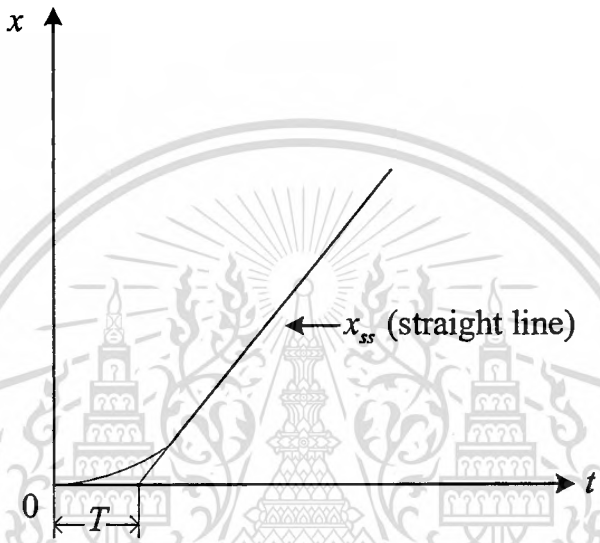

Figure 2.9 Response to a constant control input voltage V_c.

From equation (2.13) and figure 2.9, we see that

(1) The straight line x_{ss} extrapolated back to $x = 0$ and intersects the time axis at $t = T$. Thus, T can be found first.

(2) The slider mass M is generally defined by a designer since motor mounting procedure. From equation (2.11), b can be found.

(3) From the slope of the steady-state response x_{ss} $\left(\frac{k_f V_c}{b}\right)$, k_f can be found.

Therefore, the parameters of ultrasonic linear motor transfer function (2.8) can be obtained from the experiment data.

2.5 Application Fields and Development Trends

Nowadays, ultrasonic linear motors are mainly used in precise positioning stages because they economically combine unlimited stroke with highest resolution. Figure 2.10 shows several technical application areas and the operating ranges covered by today's ultrasonic linear motors.

This material is reserved for educational use only, not allowed for commercial use.
Forbidden to modify the content, and cite the document when use.

It is obvious that ultrasonic linear motors could be used as drives for storage device or other office equipments as well as in special applications like micro-robot's grippers. Some applications such as car-industry require higher thrust forces and velocities.

At present, the ultrasonic linear motors are used for micro-scale applications because their efficiency is independent on their size. Therefore, the design concept of new ultrasonic linear motor development must be optimized the following:

(1) A simple structure for which the number of components is small as possible as desired.

(2) A simple construction process.

(3) It is best to minimize the number of vibration sources and drive circuit components required for operation.

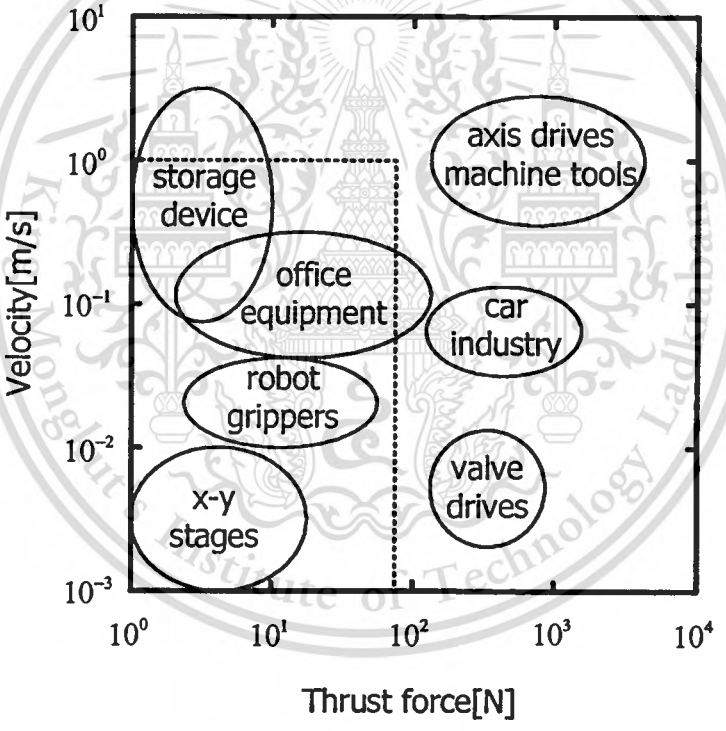

Figure 2.10 Application fields for ultrasonic linear motors.

From above requirements, the standing wave motor meets them nicely. In addition, the standing wave motor is generally less expensive because of simpler structure. This type also offers an exceptionally high efficiency. One important consideration in the design of ultrasonic linear motors concerns the support of the stator. The nodal points or lines of a standing wave motor is stationary and thus serve as ideal contact points for the support structure. The traveling wave motor will not have this feature and care must be taken in selecting and making contact with

This material is reserved for educational use only, not allowed for commercial use.
Forbidden to modify the content, and cite the document when use.

support points so that the bending vibration is not significantly suppressed. This problem precludes any further miniaturization of the traveling wave motor. Thus, no product of the linear traveling wave motors made to market until today.

This material is reserved for educational use only, not allowed for commercial use.
Forbidden to modify the content, and cite the document when use.

Chapter 3

Coefficient Diagram Method

The general problem of control system design how to choose a proper controller to meet desired performance specifications. There are three main theories employed for a design procedure: Classical Control Theory, Modern Control Theory and Polynomial Approach, which is sometimes called the Algebraic Approach. The classical control method, such as frequency response method and root-locus method, uses the transfer function for the system representation. The transfer function is easy to handle, but it becomes inaccurate when pole-zero cancellation occurs due to uncontrollable or unobservable situations. The modern control method like pole-placement method and optimal control, uses state-space representation. This representation is accurate and well-suited in machine computation. The Coefficient Diagram Method (CDM) is an algebraic control design approach. This method uses polynomials for system representation. The denominator and the numerator of the transfer function are considered independently from each other. Thus, the better results can be achieved against pole-zero cancellation. In this chapter, the CDM standard block diagram and the basic mathematical relations concerning the CDM will be described.

3.1 Basic Features of CDM

The CDM is an algebraic control design approach with the following five features.

(1) Polynomials are used for system representation.

(2) Characteristic polynomial and controller are simultaneously designed.

(3) Coefficient diagram is effectively utilized.

(4) The sufficient condition for stability by Lipatov constitutes the theoretical basis of CDM.

(5) Kessler standard form is improved and used as the standard form of CDM.

CDM design is based on the stability index γ_i and the equivalent time constant τ as defined later. The equivalent time constant τ specifies the response speed. The stability index γ_i specifies the stability and the wave form of the time response. The variation of stability index γ_i due to the plant parameter variation specifies the robustness.

This material is reserved for educational use only, not allowed for commercial use.
Forbidden to modify the content, and cite the document when use.

3.2 CDM Standard Block Diagram

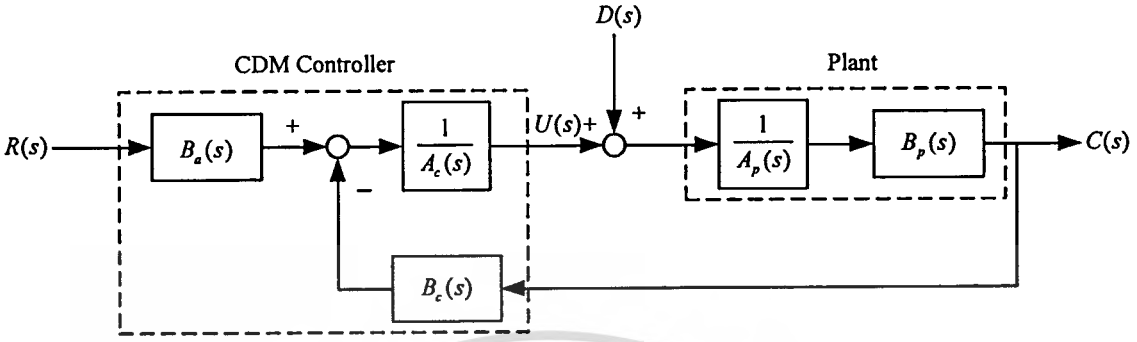

Figure 3.1 CDM standard block diagram of SISO system.

The standard block diagram of the CDM design for a single-input-single-output system is shown in figure 3.1. $A_p(s)$ and $B_p(s)$ are the polynomials of the plant, $A_c(s)$, $B_c(s)$ and $B_a(s)$ are the polynomials of the standard CDM controller. $D(s)$ is the disturbance entering to the controlled system. The transfer function of the plant in polynomial form can be expressed as

$$A_p(s) = p_k s^k + p_{k-1} s^{k-1} + \ldots + p_0 \tag{3.1}$$

$$B_p(s) = q_m s^m + q_{m-1} s^{m-1} + \ldots + q_0 \tag{3.2}$$

and the controller polynomials are given by

$$A_c(s) = l_\lambda s^\lambda + l_{\lambda-1} s^{\lambda-1} + \ldots + l_0 \tag{3.3}$$

$$B_c(s) = k_\lambda s^\lambda + k_{\lambda-1} s^{\lambda-1} + \ldots + k_0 \tag{3.4}$$

$$B_a(s) = p_\lambda s^\lambda + p_{\lambda-1} s^{\lambda-1} + \ldots + p_0 \tag{3.5}$$

where $\lambda < k$ and $m < k$. $B_a(s)$ is called pre-filter. Since the transfer function of the controller has two numerators, it is resembled to a two-degree-of freedom (2DOF) system structure.

This material is reserved for educational use only, not allowed for commercial use.
Forbidden to modify the content, and cite the document when use.

The better performance can be expected when using 2DOF structure, because it can compromise on both tracking the desired reference signal and disturbance suppression.

3.3 Characteristic Polynomial

The characteristic polynomial of the closed-loop system without pre-filter is defined as

$$P(s) = A_c(s)A_p(s) + B_c(s)B_p(s)$$

$$= a_n s^n + a_{n-1}s^{n-1} + \ldots + a_1 s + a_0 \tag{3.6}$$

$$= \sum_{i=0}^{n} a_i s^i$$

where $a_0, a_1, \ldots, a_n$ are the coefficients of the characteristic polynomial. The stability index γ_i, the equivalent time constant τ and stability limit γ_i^* are defined as follows.

$$\gamma_i = \frac{a_i^2}{a_{i+1}a_{i-1}} \tag{3.7}$$

$$\tau = \frac{a_1}{a_0} \tag{3.8}$$

$$\gamma_i^* = \frac{1}{\gamma_{i+1}} + \frac{1}{\gamma_{i-1}}; \gamma_0, \gamma_n = \infty \tag{3.9}$$

where $i = 1, \ldots, n-1$. From (3.7) and (3.8), the coefficient a_i can be written by

$$a_i = a_0 \tau^i \frac{1}{\gamma_{i-1} \cdots \gamma_2^{i-2} \gamma_1^{i-1}}$$

$$= a_0 \tau^i \prod_{j=1}^{i-1} \frac{1}{\left(\gamma_{i-j}\right)^j}. \tag{3.10}$$

This material is reserved for educational use only, not allowed for commercial use.
Forbidden to modify the content, and cite the document when use.

Substituting each coefficient a_i into equation (3.6), then the characteristic polynomial will be expressed in term of a_0, τ and γ_i as

$$P(s) = a_0\left[\left\{\sum_{i=2}^{n}\left(\prod_{j=1}^{i-1}\frac{1}{\gamma_{i-j}^{j}}\right)(\tau s)^i\right\}+\tau s+1\right]. \tag{3.11}$$

3.4 Coefficient Diagram

Coefficient diagram is a powerful and useful tool for the controller design. It gives information on stability, time response and robustness of systems in a single diagram. In coefficient diagram, vertical axis logarithmically shows the coefficients of characteristic polynomial a_i, stability index γ_i, stability limits γ_i^* and equivalent time constant τ while the horizontal axis shows the order i values corresponding to each coefficient. The degree of convexity is a measure of stability. The general inclination of the curve is a measure of response speed. The variation of the shape of the curve due to the plant parameter variation is a measure of robustness.

To give an idea about the coefficient diagram consider the characteristic polynomial

$$P(s) = 0.25s^5 + s^4 + 2s^3 + 2s^2 + s + 0.2 \tag{3.12}$$

for the following CDM parameters

$$\gamma_i = [2\ 2\ 2\ 2.5] \tag{3.13}$$

$$\tau = 5 \tag{3.14}$$

$$\gamma_i^* = [0.5\ 1\ 0.9\ 0.5]. \tag{3.15}$$

These values are shown in a coefficient diagram as in figure 3.2. The control system becomes more stable if the curvature of the a_i curve becomes larger corresponding to larger stability index γ_i as shown in figure 3.3a. If the a_i curve is left-end down, the equivalent time constant τ is small and response is fast as shown in figure 3.3b.

This material is reserved for educational use only, not allowed for commercial use.
Forbidden to modify the content, and cite the document when use.

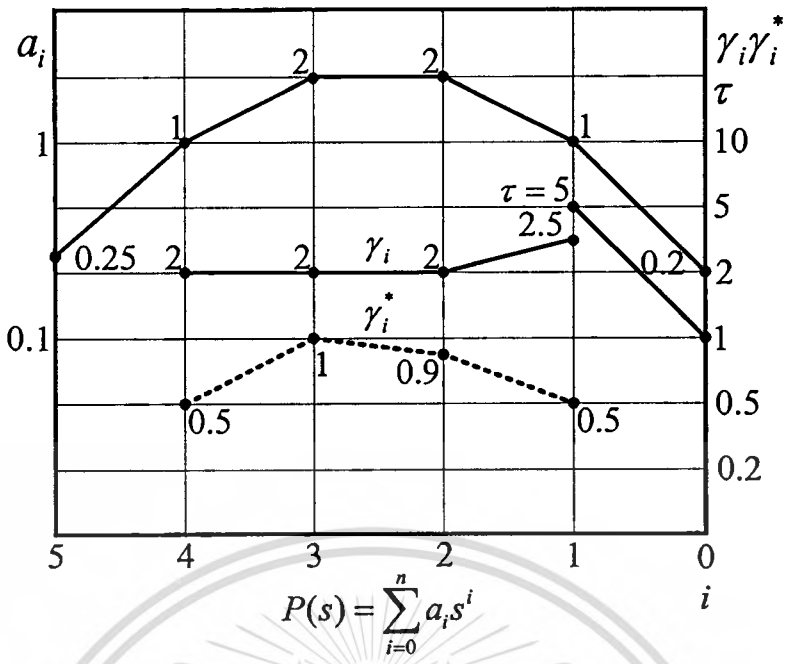

Figure 3.2 Coefficient diagram.

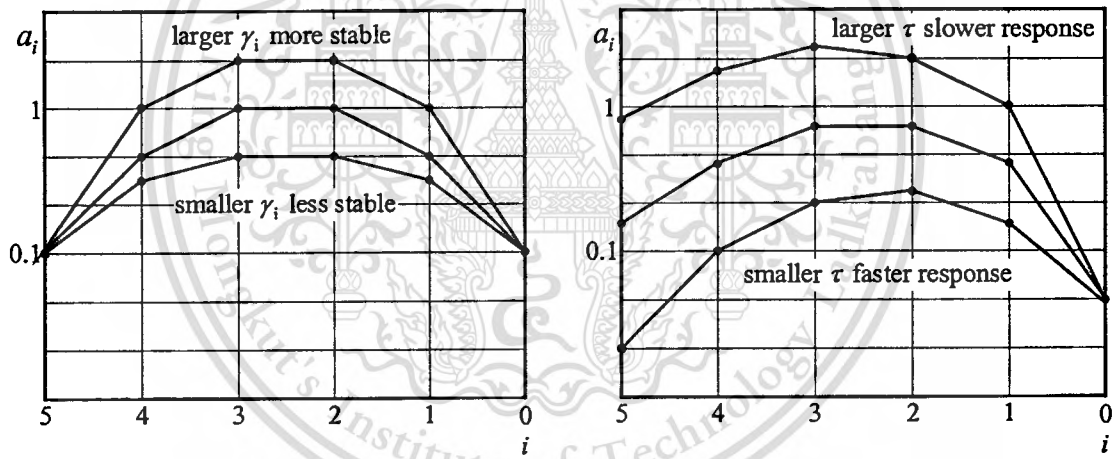

(a) system stability **(b)** system response

Figure 3.3 Variation of stability index γ_i corresponding to system stability and system response.

3.5 Stability Condition

Stability analysis of systems with the third or fourth order characteristic polynomial can easily be done using Routh-Hurwitz stability criterion. However, the effect of coefficient variations on stability cannot be seen clearly for systems with higher orders. Necessary conditions for stability or instability of systems with higher orders can be found easily using Lipatov's work.

This material is reserved for educational use only, not allowed for commercial use.
Forbidden to modify the content, and cite the document when use.

From the Routh-Hurwitz stability criterion, the stability condition for the third order is given as

$$a_2 a_1 > a_3 a_0 . \tag{3.16}$$

If it is expressed by stability index γ_i,

$$\gamma_2 \gamma_1 > 1 . \tag{3.17}$$

The stability condition for the fourth order is given as

$$a_2 > (a_1/a_3) a_4 + (a_3/a_1) a_0, \tag{3.18}$$

$$\gamma_2 \gamma_3 > 1 . \tag{3.19}$$

Form equations (3.9), (3.17) and (3.19), it is concluded that the stability condition for the third and fourth order is written by

$$\gamma_i > \gamma_i^* , \text{ for all } i = 2 \sim n-2 . \tag{3.20}$$

For the system higher than or including the fifth order, Lipatov gave the sufficient condition for stability and instability in several forms. The conditions most suitable to CDM can be stated as follows;

"The system is stable, if all the partial fourth-order polynomials are stable with the margin of 1.12. The system is unstable if some partial third-order polynomial is unstable."

Thus the sufficient condition for stability is given as

$$a_i > 1.12 \left(\frac{a_{i-1}}{a_{i+1}} a_{i+2} + \frac{a_{i+1}}{a_{i-1}} a_{i-2} \right) , \tag{3.21}$$

$$\gamma_i > 1.12 \gamma_i^* , \text{ for all } i = 2 \sim n-2 . \tag{3.22}$$

This material is reserved for educational use only, not allowed for commercial use.
Forbidden to modify the content, and cite the document when use.

The sufficient condition for instability is given as

$$a_{i+1}a_i \le a_{i+2}a_{i-1}, \tag{3.23}$$

$$\gamma_{i+1}\gamma_i \le 1, \text{ for some } i = 1 \sim n-2. \tag{3.24}$$

3.6 Standard Form of CDM

Kessler proposed stability index γ_i to be 2 for all i in order to decrease the oscillation and overshoot in the ITAE (Integral Time Absolute Error) form. But it was later found that better response, no overshoot and shorter settling time can be obtained by increasing γ_1 to 2.5. Thus the standard value of γ_i for the CDM is

$$\gamma_{n-1} = \ldots = \gamma_3 = \gamma_2 = 2, \quad \gamma_1 = 2.5, \tag{3.25}$$

and CDM design has a settling time

$$t_s = 2.5\tau \sim 3\tau. \tag{3.26}$$

As in equation (3.11), the characteristic polynomial is expressed in the powers of τs, and the coefficients are expressed by γ_i. Thus the shapes of response and speed are determined by γ_i and τ respectively.

The features of the CDM standard form can be summarized as follow:

(1) No overshoot for the type 1 system, and a proper overshoot about 40 percent for the type 2 system

(2) The shortest settling time for the same equivalent time constant τ

(3) The similar wave form irrespective to the order of system

(4) The low order poles are of the equal decay. The high order poles are in the sector ± 50 degrees from the negative real axis. The damping ratio ζ is 0.65.

This material is reserved for educational use only, not allowed for commercial use.
Forbidden to modify the content, and cite the document when use.

3.7 Modification of the CDM Standard Form

In the actual design, the choice of the standard stability index is strongly recommended due to stability and response requirements. However, it is not necessary to make $\gamma_4 \sim \gamma_{n-1}$ equal to 2. The condition can be relaxed as

$$\gamma_i > 1.5\gamma_i^* . \tag{3.27}$$

Therefore, the designer has the freedom of designing the controller. Sometimes it may be advisable to select the larger value of the stability index, in order to improve the robustness related parameter change. From the sufficient condition for stability by Lipatov, stability is guaranteed when all γ_i's are larger than 1.5. Lipatov proved in his paper [19] that, if all γ_i's are greater than 4, all the roots are negative real. Thus, γ_i's are usually chosen between 1.5 and 4. Sometimes the system is built in such manner that some γ_i is already larger than the standard value. In such case it is not necessary to reduce it to the standard value.

This material is reserved for educational use only, not allowed for commercial use.
Forbidden to modify the content, and cite the document when use.

Chapter 4

Design of PDFF Controller by CDM

A designing method of the PDFF controller by CDM to meet desired performance criteria is discussed in this chapter. The parameters of PDFF controller are designed based on the stability and the speed of the controlled system. Stability is designed from the standard stability index γ_i, and speed is designed from the equivalent time constant τ and the tuning factor α. The stability index γ_i, the equivalent time constant τ, and the tuning factor α are defined based on the closed-loop transfer function. These coefficients are related to the controller parameters algebraically in an explicit form. According to the design methodology of the CDM, the parameters of the PDFF controller can be obtained easily and properly.

4.1 Control System Structure

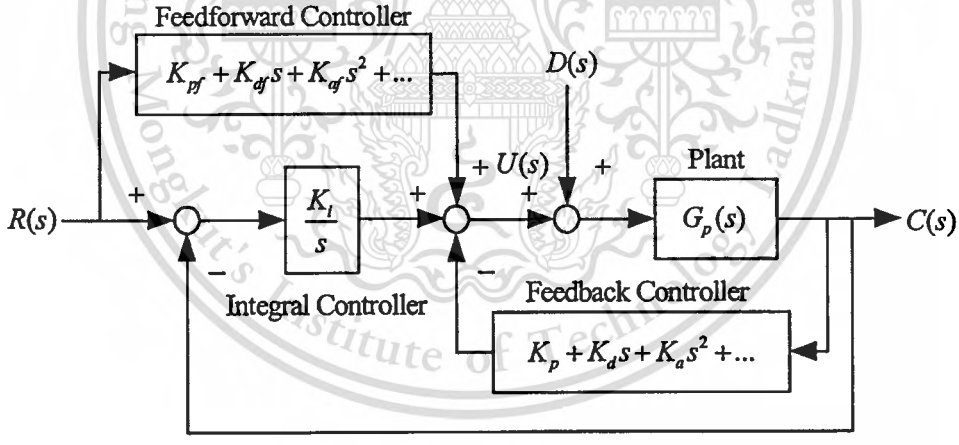

Figure 4.1 General PDFF control system structure.

The general PDFF control system structure shown in figure 4.1 consists of a plant, a feedforward controller, a feedback controller and an integral controller. In order to use CDM to design the PDFF controller parameters properly, the PDFF control system in the form of CDM consisting of the CDM standard block diagram of SISO system with the feedforward and feedback controllers is proposed (see figure 4.2). The controllers and the plant must be represented by polynomials. $A_p(s)$ and $B_p(s)$ are the polynomials of the plant $G_p(s)$, $A_c(s)$,

This material is reserved for educational use only, not allowed for commercial use.
Forbidden to modify the content, and cite the document when use.

$B_c(s)$ and $B_a(s)$ are the polynomials of the standard CDM controller, $B_{ff}(s)$ is the polynomial of the feedforward controller, and $B_{fb}(s)$ is the polynomial of the feedback controller. $D(s)$ is the disturbance entering to the controlled system.

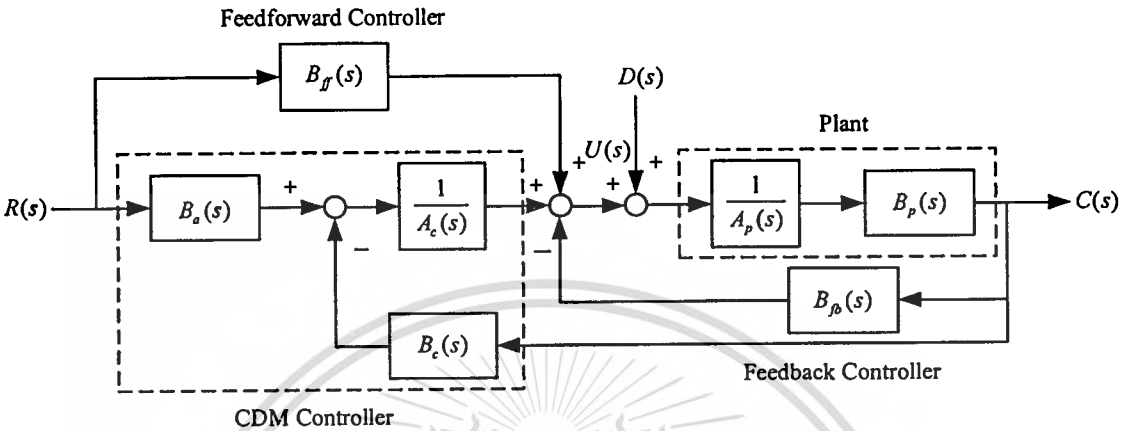

Figure 4.2 PDFF control system in the form of CDM.

The polynomials of the modified plant $A_p^*(s)$ and $B_p^*(s)$ shown in figure 4.3 are obtained from plant $G_p(s)$ and feedback controller $B_{fb}(s)$.

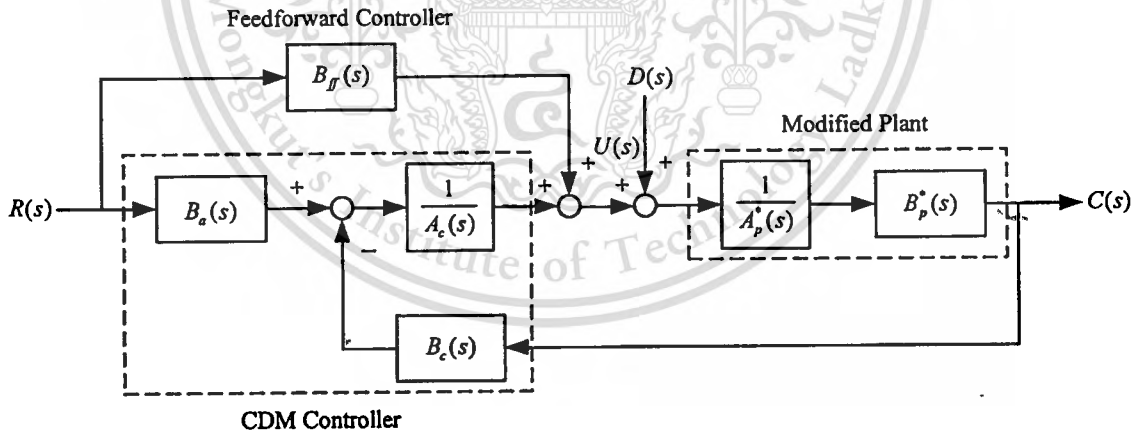

Figure 4.3 Rearranged structure of figure 4.2.

From the block diagram of figure 4.3, The transfer function from $R(s)$ to $C(s)$ is then given by

$$\frac{C(s)}{R(s)} = \frac{B_p^*(s)\ B_a(s) + B_{ff}(s)A_c(s)}{A_c(s)A_p^*(s) + B_c(s)B_p^*(s)}, \tag{4.1}$$

and the transfer function between $D(s)$ and $C(s)$ is

This material is reserved for educational use only, not allowed for commercial use.
Forbidden to modify the content, and cite the document when use.

$$\frac{C(s)}{D(s)} = \frac{B_p^*(s)A_c(s)}{A_c(s)A_p^*(s) + B_c(s)B_p^*(s)}. \tag{4.2}$$

From the transfer functions (4.1) and (4.2), it is seen that the feedforward controller $B_{ff}(s)$ has an influence on the transfer function from $R(s)$ to $C(s)$ and can be used to increase the speed of the transient response of the controlled system, while the transfer function from $D(s)$ to $C(s)$ is not affected.

In order to derive the closed-loop transfer function of PDFF control system in term of γ_i, τ and α, the closed-loop transfer function given by equation (4.1) may be expressed by

$$\frac{C(s)}{R(s)} = \frac{B(s)}{A(s)}$$

$$= \frac{b_m s^m + b_{m-1}s^{m-1} + \ldots + b_1 s + b_0}{a_n s^n + a_{n-1}s^{n-1} + \ldots + a_1 s + a_0}, \tag{4.3}$$

where $m \le n$, and a's and b's are constants. The denominator polynomial $A(s)$ is the characteristic polynomial of the closed-loop system, and its coefficients can be found from

$$A(s) = a_0\left[\left\{\sum_{i=2}^{n}\left(\prod_{j=1}^{i-1}\frac{1}{\gamma_{i-j}^{j}}\right)(\tau s)^i\right\} + \tau s + 1\right]. \tag{4.4}$$

This equation is the same form of equation (3.1).

The CDM is mainly used to design the characteristic polynomial of the closed-loop system. However, this method can be extended to design the coefficients of the numerator polynomial $B(s)$ as well [15],[20]. Thus, the relationship among the coefficients of the numerator polynomial $B(s)$ can be written by

$$b_i = b_0(\alpha\tau)^i \frac{1}{\gamma_{i-1}\cdots\gamma_2^{i-2}\gamma_1^{i-1}}$$

$$= b_0(\alpha\tau)^i \prod_{j=1}^{i-1}\frac{1}{\left(\gamma_{i-j}\right)^j}, \tag{4.5}$$

This material is reserved for educational use only, not allowed for commercial use.
Forbidden to modify the content, and cite the document when use.

where α is the tuning factor. The equivalent time constant τ is scaled by the tuning factor α so that the response speed can be adjusted. The value of tuning factor α is defined as $0<\alpha\leq 1$. Substituting each coefficient b_i into the numerator polynomial $B(s)$, which is expressed in term of γ_i, τ and α as

$$B(s)=b_0\left[\left\{\sum_{i=2}^{m}\left(\prod_{j=1}^{i-1}\frac{1}{\gamma_{i-j}^{j}}\right)(\alpha\tau s)^i\right\}+\alpha\tau s+1\right]. \tag{4.6}$$

Hence, the transfer function of PDFF control system in term of γ_i, τ and α can be obtained by

$$\frac{C(s)}{R(s)}=\frac{b_0\left[\left\{\sum_{i=2}^{m}\left(\prod_{j=1}^{i-1}\frac{1}{\gamma_{i-j}^{j}}\right)(\alpha\tau s)^i\right\}+\alpha\tau s+1\right]}{a_0\left[\left\{\sum_{i=2}^{n}\left(\prod_{j=1}^{i-1}\frac{1}{\gamma_{i-j}^{j}}\right)(\tau s)^i\right\}+\tau s+1\right]}. \tag{4.7}$$

This transfer function is a general form for designing the PDFF controller.

4.2 Design Procedure

The parameters of PDFF controller can be designed by following procedures:

(1) Derive the closed-loop transfer function (4.1) from the polynomials of the modified plant, the feedforward controller, the integral controller and the pre-filter.

(2) Define the settling time t_s in order to find the equivalent time constant τ from equation (3.26), and determine the proper values of stability index γ_i and tuning factor α. Then, substituting these parameters to the closed-loop transfer function (4.7).

(3) The parameters of PDFF controller are obtained by equating the transfer function (4.1) to the transfer function (4.7).

4.3 PDFF Controller Design for Position Control of Ultrasonic Linear Motor

Since the model of ultrasonic linear motor is approximated to be a second-order system, the structures of feedforward and feedback controllers shown in figure 4.1 become as proportional-derivative control actions as shown in figure 4.4. K_d and K_p are the derivative and proportional

This material is reserved for educational use only, not allowed for commercial use.
Forbidden to modify the content, and cite the document when use.

gains of feedback controller respectively, K_i is the integral gain, and K_{df} and K_{pf} are the derivative and proportional gains of feedforward controller respectively.

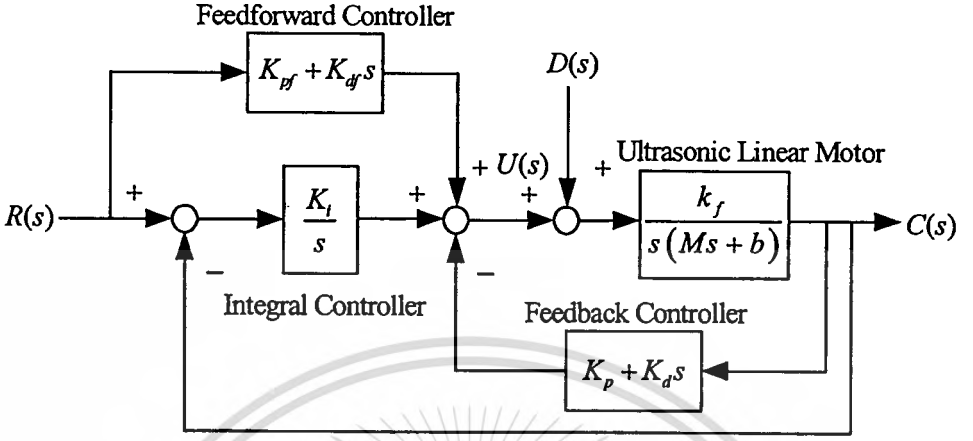

Figure 4.4 Ultrasonic linear motor with PDFF controller.

To assign the parameters of the feedforward controller, the feedback controller and the integral controller, the transfer function (4.1) must be first found from the modified plant

$$G_p^*(s)=\frac{B_p^*(s)}{A_p^*(s)}=\frac{B_p(s)}{A_p+\left(K_p+K_ds\right)B_p(s)}, \tag{4.10}$$

the integral controller

$$G_c(s)=\frac{B_c(s)}{A_c(s)}=\frac{K_i}{s}, \tag{4.11}$$

the feedforward controller

$$B_{ff}(s)=K_{df}s+K_{pf}, \tag{4.12}$$

and the pre-filter

$$B_a(s)=K_i, \tag{4.13}$$

This material is reserved for educational use only, not allowed for commercial use.
Forbidden to modify the content, and cite the document when use.

CHAPTER 3

BACKGROUND OF ZINC OXIDE (ZnO)

3.1 Introduction to ZnO

ZnO is of particular interest due to its wide band gap and excellent optical qualities, making it a promising material for several applications such as ultraviolet optoelectronics, transparent contacts, varistors and gas sensors. It is also nearly identical in lattice spacing to GaN, meaning that integration of ZnO with GaN based systems is possible. The major difficulty in producing ZnO devices is the lack of *p*-type doping. As grown, ZnO is n-type due to structural defects from the growth process, such as oxygen vacancies, zinc interstitials and anti-sites. An anti-site occurs when a nucleus of one species occupies a lattice site that is typically occupied by another species, such as a zinc nucleus on an oxygen site in the lattice. A vacancy is an unoccupied lattice site, resulting in unsatisfied bonds within the lattice. An interstitial defect is a nucleus that does not occupy a lattice site, perturbing the periodic potential that gives rise to the ideal band structure.

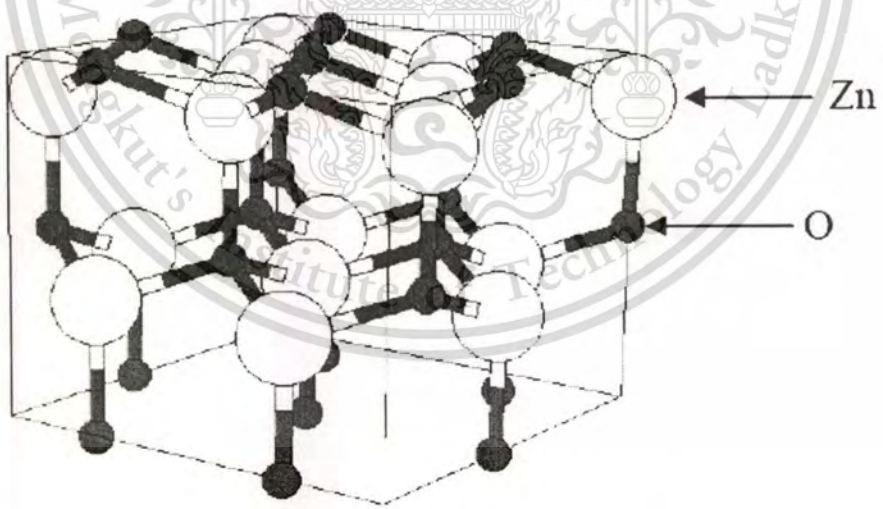

Fig. 3.1 Crystalline ZnO forms in the wurtzite structure [1].

The ideal band structure of a semiconductor is born out of the periodicity of a crystal lattice, and the periodic electric potential associated with it. Any deviation from an ideal, periodic

This material is reserved for educational use only, not allowed for commercial use.
Forbidden to modify the content, and cite the document when use.

Chapter 5

Simulation and Experimental Results

The effectiveness of the PDFF controller developed for the position control of ultrasonic linear motor will be evaluated in this chapter. A series of simulations and experiments are performed. The PDFF control algorithm is first used to study the system response at a desired constant position value, and then, to study the disturbance rejection capability. Finally, the system response in a tracking mode will be regarded.

5.1 Experimental System

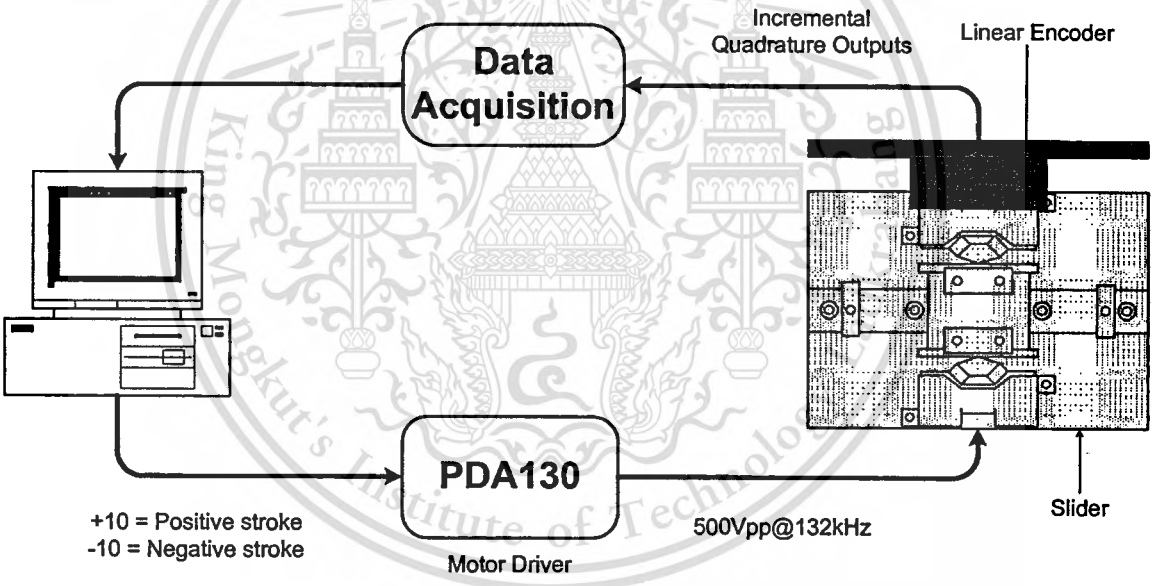

Figure 5.1 Experimental system.

The experimental system of position control for ultrasonic linear motor is set up as shown in figure 5.1. The structure of ultrasonic linear motor consists of two piezoelectric actuators, a linear bearing and a slider plate. In this work, two piezoelectric actuators model PDM130 are used as stators to increase the thrust force. The piezoelectric actuator structure and its electrical schematic are shown in figures 5.2 and 5.3 respectively. To obtain a very low friction slide mechanism, each piezoelectric actuators is installed on a side of linear bearing as shown in figure 5.4. The friction shoe is coupled to flat friction strip which is mounted on a side of bearing using double sided

This material is reserved for educational use only. Not allowed for commercial use.
Forbidden to modify the content, and cite the document when use.

adhesive tape. A slider plate is mounted on the linear bearing, and its weight is 0.12 kg. The friction drive of the actuator (stator) requires a compressive pre-load force between the friction shoe and the friction strip. The pre-load force is determined by spring compression, which is determined by the mounting distance between the actuator housing and friction strip. In this case, the motor mounting distance is 0.24 inches for fast speed requirement [21].

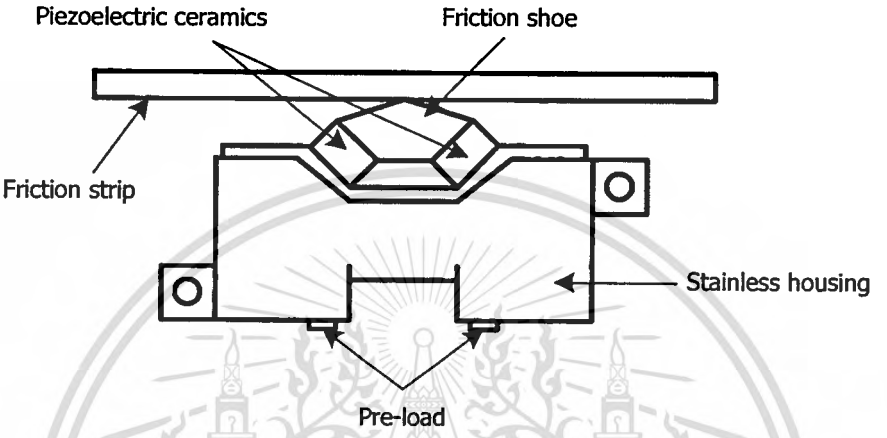

Figure 5.2 Structure of PDM130.

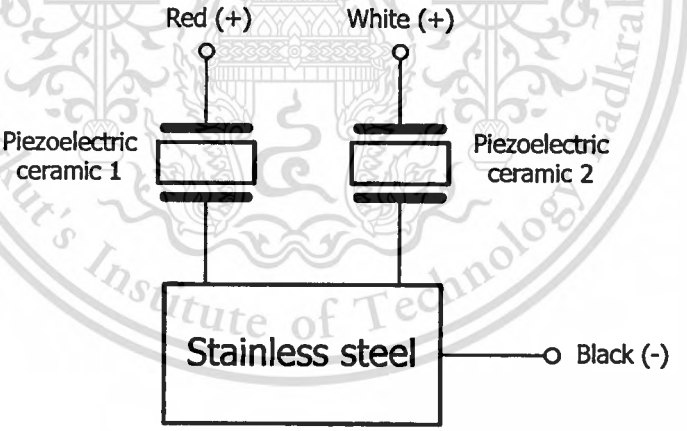

Figure 5.3 Electrical schematic of PDM130.

The ultrasonic linear motor is driven by standard motor driver model PDE130. This driver provides 500 Vpp to the motor at a driving frequency of approximately 132 kHz. Motor driver is controlled using –10 to +10 control input voltage from the personal computer. The voltage sign controls the motor direction and the voltage magnitude controls the motor speed. The actual position of slider is detected by linear encoder, whose incremental quadrature outputs provide 5 μ m measuring steps. The maximum stroke of slider is about 40 mm.

Forbidden to modify the content, and cite the document when use.

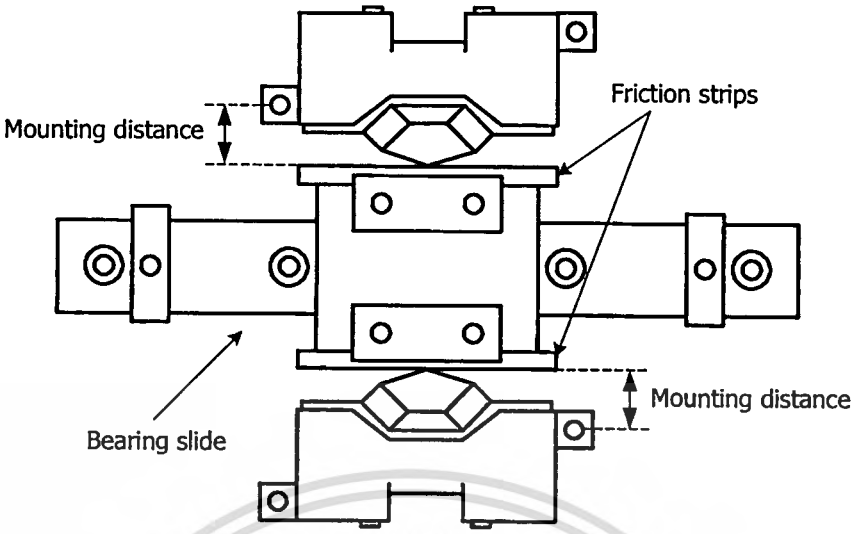

Figure 5.4 Structure of ultrasonic linear motor (top view).

5.2 PDFF Controller Parameters

The parameters of PDFF controller have to be assigned for simulations and experiments. Hence, the parameters of the ultrasonic linear motor model are first determined from experimental data based on the technique described in chapter 2. Applying the +10 V control input voltage from personal computer to the ultrasonic linear motor through the motor driver PDA130, the open-loop response of ultrasonic linear motor can be obtained (see figure 5.5).

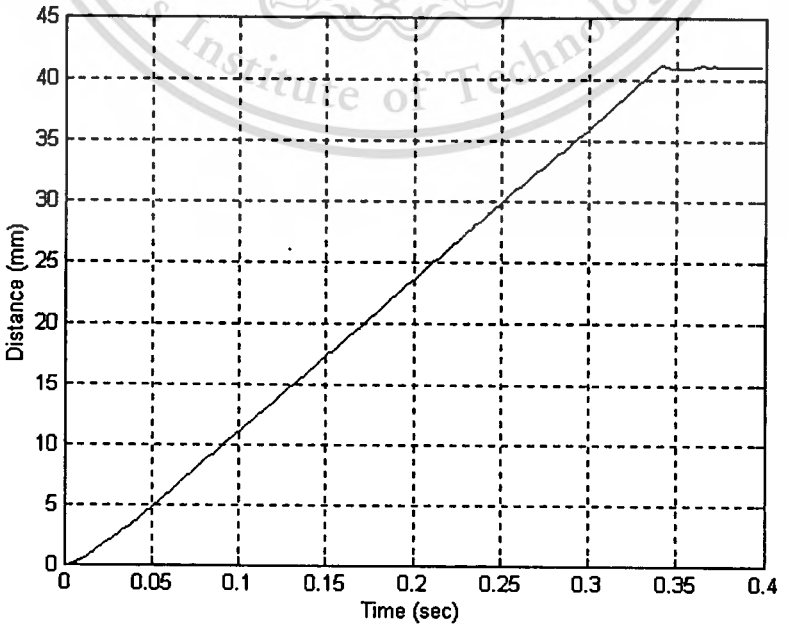

Figure 5.5 Open-loop response.

This material is reserved for [illegible] owed for commercial use.
Forbidden to modify the content, and cite the document when use.

From the open-loop response curve, the slope of the steady-state response is 0.116, the straight line of steady-state response extrapolated back to the time axis and intersects this axis at 0.006 second. Thus, its model can be found as

$$G_p(s) = \frac{0.23}{s(0.12s + 19.88)},$$

where the input of this model is the control input voltage V_{in}, and the output is the position of slider $X(s)$.

In actual operation, the load mass on the slider can be changed up to applications which leads to the model parameters change. Hence, the controller parameters should be designed by large stability index value. In this work, the controller parameters are designed by setting the stability indices $\gamma_1 = 7$ and $\gamma_2 = 15$, the equivalent time constant $\tau = 0.6$ second, for the settling time $t_s = 1.5$ seconds, and the tuning factor α is 0.6 (see Appendix B). Thus, the parameters of PDFF controller obtained from the design procedure stated in chapter 4 are $K_p = 1061.66$, $K_i = 1769.44$, $K_d = 4.57$, $K_{pf} = 637.00$ and $K_{df} = 32.76$.

5.3 Simulation Results

5.3.1 Step Response of Position Control

The simulations of the PDFF control system shown in figure 4.2 for a 20mm step input with no load mass and its control signal are shown in figures 5.6 and 5.7 respectively. It is seen that the response has no steady-state error and overshoot. A rise time and a settling time are shown in table 5.1. Since the model of ultrasonic linear motor is the second-order system and the system type is one, it is possible to use the PD controller to control the position of the motor. Therefore, in this work, the PD position control system (see Appendix D) is also designed to compare the results with the PDFF control system. The both control systems have the same settling time, but the rise time of PDFF control system is shorter.

Table 5.1 System performance comparison (simulations)

Operating condition	t_r (sec)	P_o (%)	t_s (sec)
No load	0.59	0.00	1.41
Load (0.5kg)	0.56	0.00	1.43

This thesis is reserved for educational use only, not allowed for commercial use.
Forbidden to modify the content, and cite the document when use.

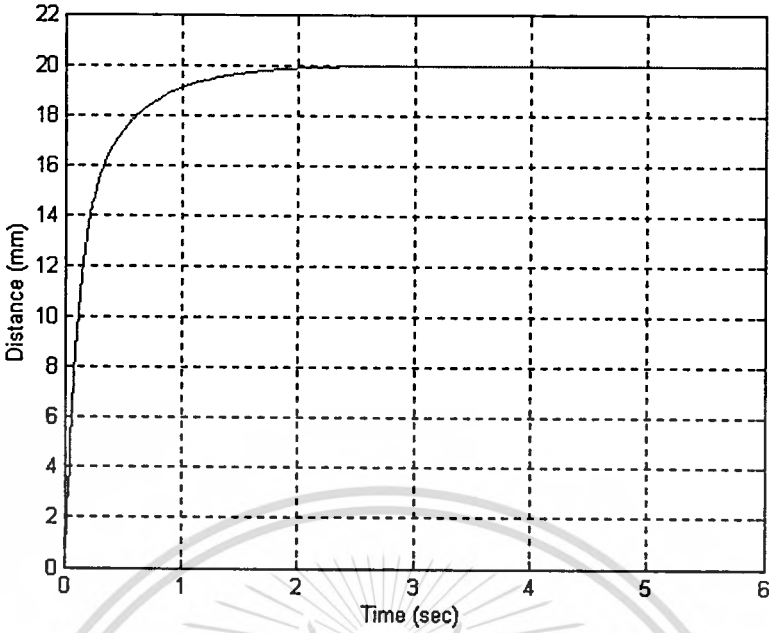

Figure 5.6 Response to step input with no load mass.

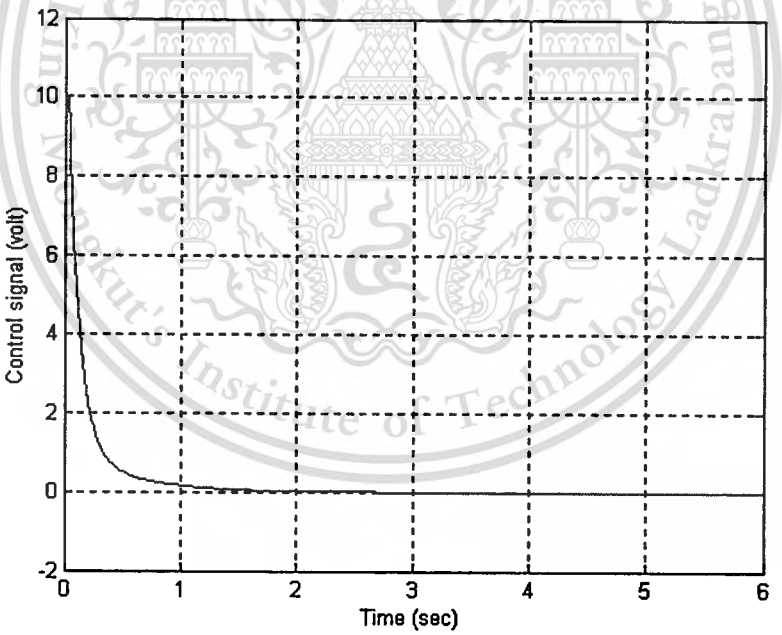

Figure 5.7 Control signal.

In order to demonstrate the effectiveness of the PDFF controller, the 0.5kg load mass is placed on the slider without changing the controller parameters. The system response for the same 20mm step input can be shown in figure 5.8, and figure 5.9 shows its control signal. There is no overshoot or steady-state error. It is seen from table 5.1 that the rise time of load condition is

This material is reserved for educational use only, not allowed for commercial use.
Forbidden to modify the content, and cite the document when use.

shorter than the rise time of no-load condition, on the other hand, the settling time of no-load condition is faster.

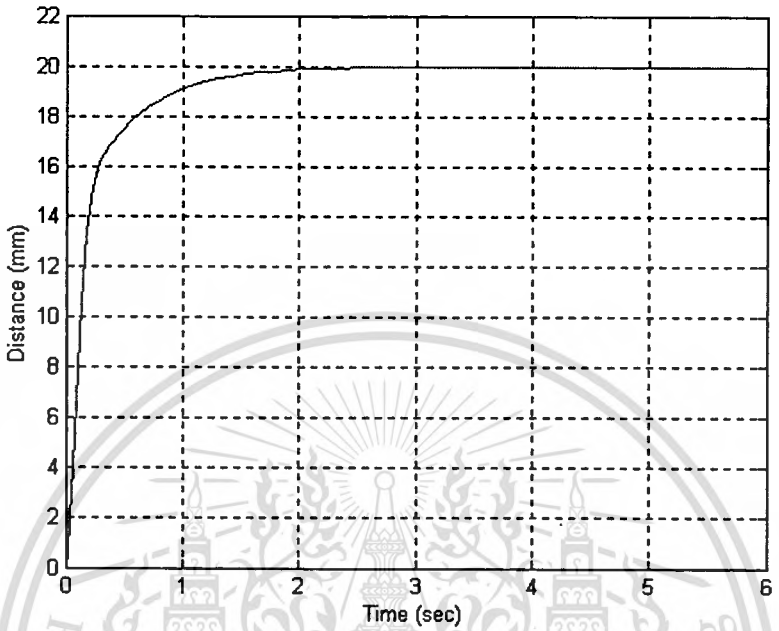

Figure 5.8 Response to step input with 0.5kg load mass.

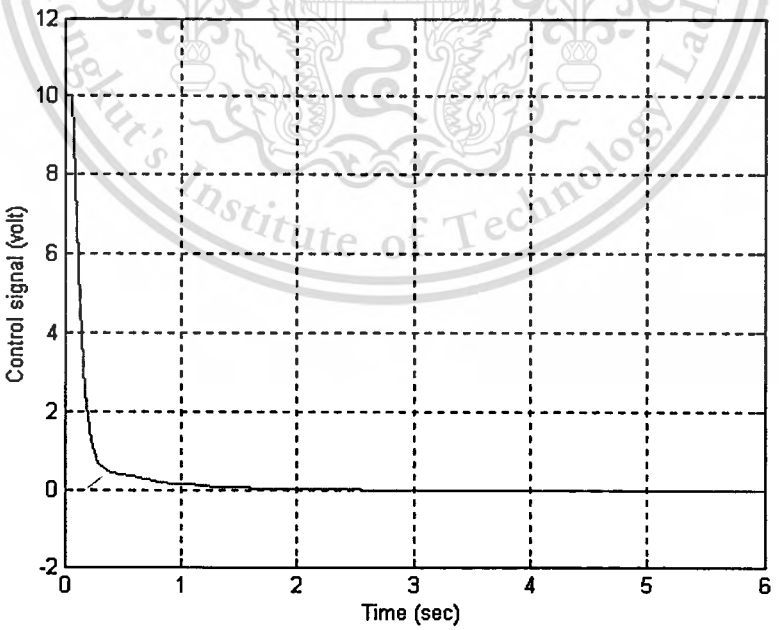

Figure 5.9 Control signal.

This material is reserved for educational use only, not allowed for commercial use.
Forbidden to modify the content, and cite the document when use.

It is obviously observed from these figures that the response curve of no-load condition is almost identical with the response curve of 0.5kg-load condition. Thus, it can be concluded that the PDFF control system designed for no-load condition still give a good response at the load condition.

5.3.2 Step Response with Constant Disturbance

The disturbance rejection capability is also examined in this work. A step disturbance equivalent to 1N is applied to the system of figure 4.2 at 6 seconds, while PDFF control system is controlling the position at 20mm. The response and the control signal are shown in figures 5.10 and 5.11 respectively. It is observed from these figures that the PDFF control system can rapidly correct the position error caused by the disturbance. However, the position error still remains in the PD control system (see Appendix D).

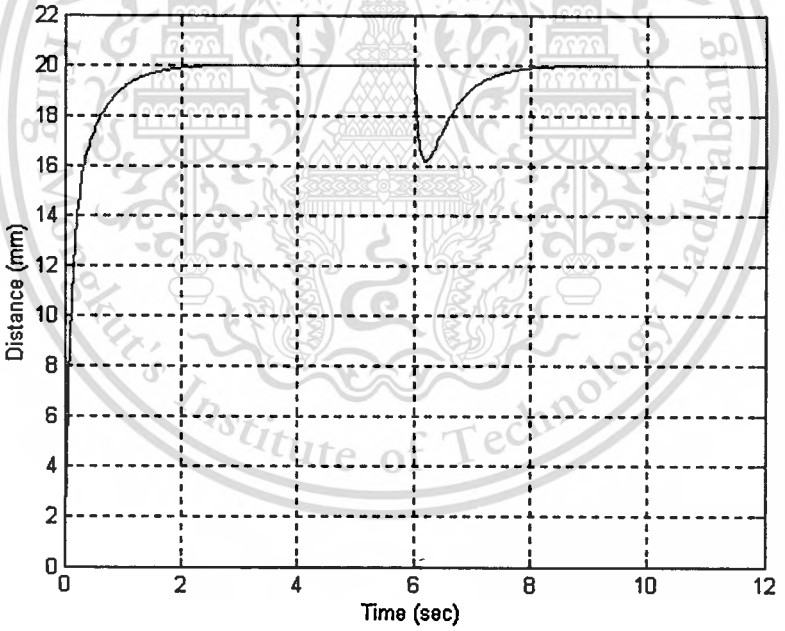

Figure 5.10 Response to step input and step disturbance.

This material is reserved for educational use only, not allowed for commercial use.
Forbidden to modify the content, and cite the document when use.

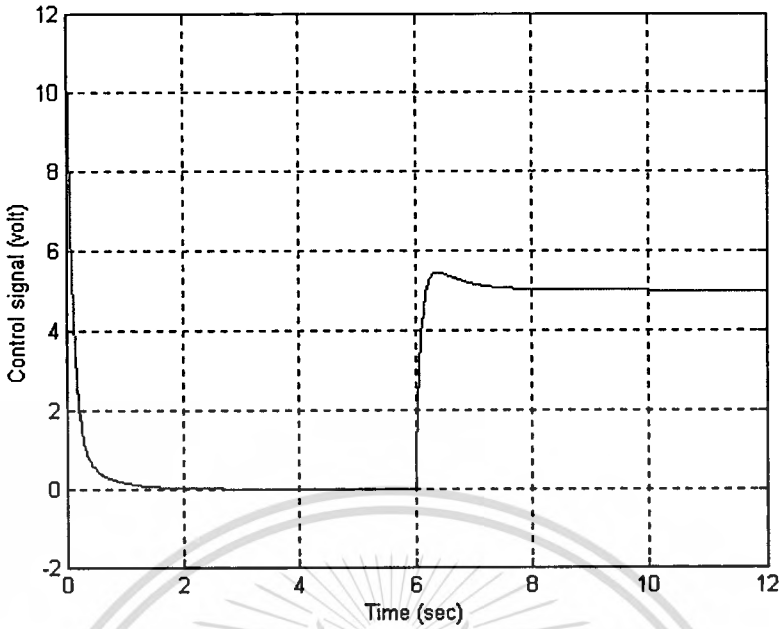

Figure 5.11 Control signal.

5.3.3 Tracking Characteristic

In this sub-section, the responses of the position control system in a tracking mode are considered both no-load and load conditions. A stair input, of which each time interval is 4 seconds for the displacement of 10mm is applied to $R(s)$ of block diagram of figure 4.2.

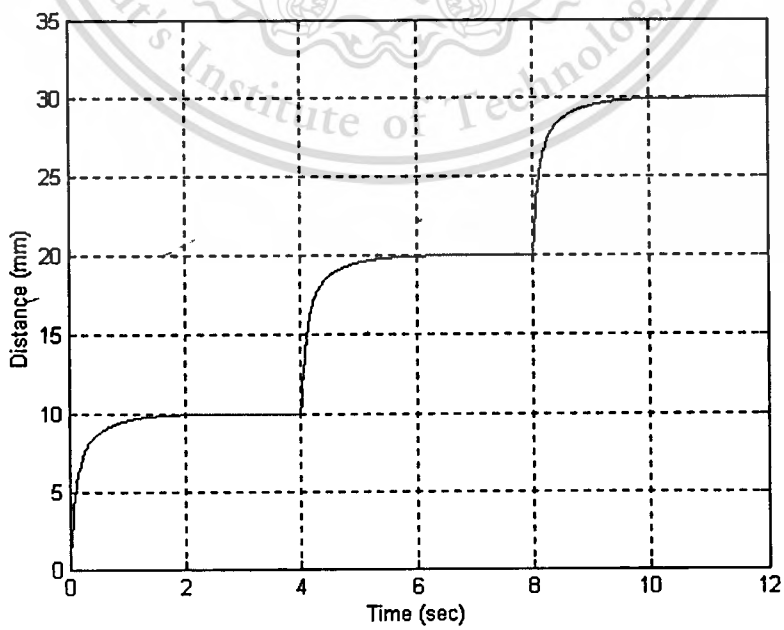

Figure 5.12 Response to stair input with no load mass.

This material is reserved for educational use only, not allowed for commercial use.
Forbidden to modify the content, and cite the document when use.

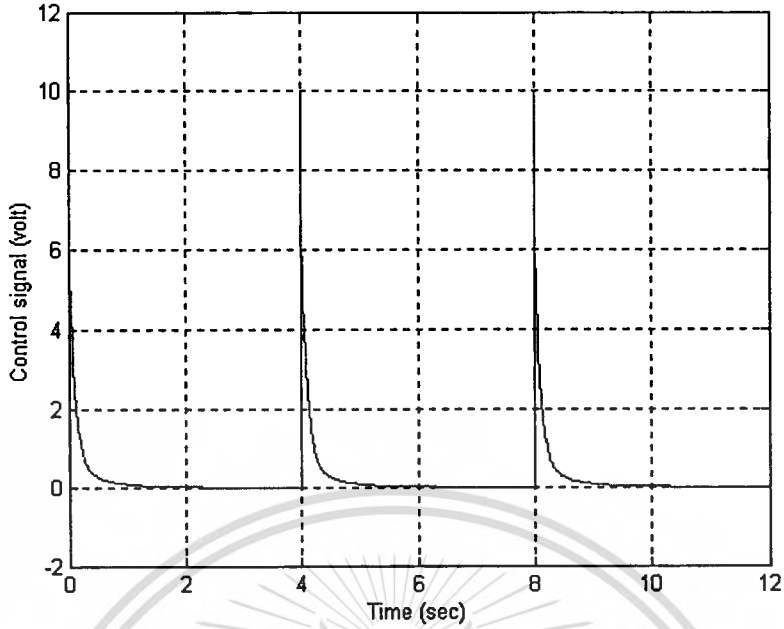

Figure 5.13 Control signal.

The simulation response for no-load condition is shown in figure 5.12, and its control signal is also shown in figure 5.13. The response can track the command positions, even if the command changes in a step without overshoot.

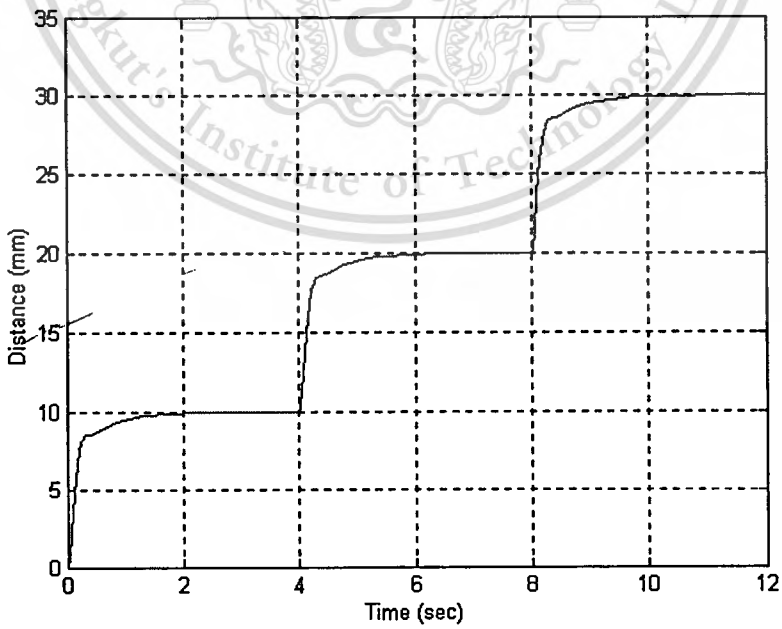

Figure 5.14 Response to stair input with 1kg load mass.

This material is reserved for educational use only, not allowed for commercial use.
Forbidden to modify the content, and cite the document when use.

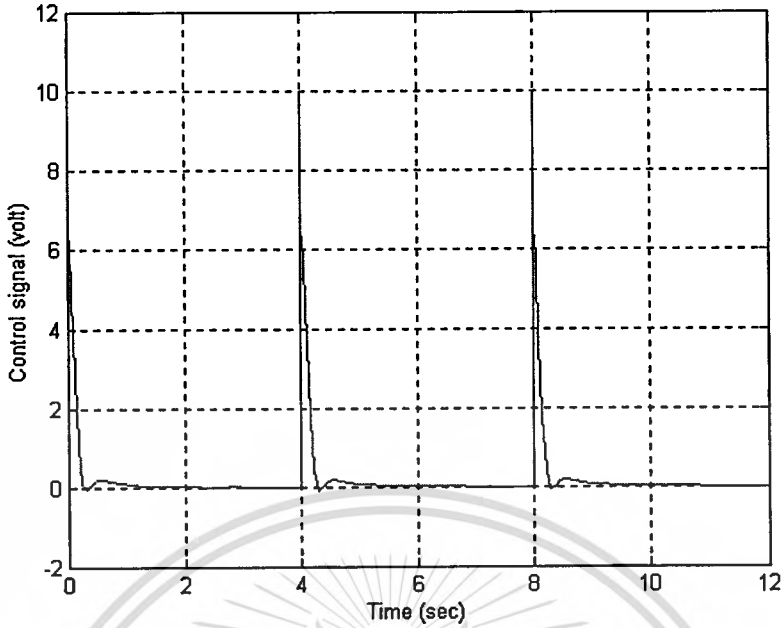

Figure 5.15 Control signal.

In case of load condition, the 1kg load mass is placed on the slider, while still using the same controller parameters designed for no-load condition. The response to the stair input and its control signal are shown in figures 5.14 and 5.15 respectively. Although, the slider carries the 1kg load mass, the PDFF controller can control the slider to the desired positions. Hence, it can be summarized that the precise and quick position tracking can be obtained from the proposed control system.

This material is reserved for educational use only, not allowed for commercial use.
Forbidden to modify the content, and cite the document when use.

5.4 Experimental Results

In this section, the experiments will be carried out to verify the effectiveness of the PDFF position control system of the ultrasonic linear motor. The photograph of the ultrasonic linear motor including the linear encoder is shown in figure 5.16. The PDFF controller algorithm is implemented with a personal computer by using C language, and the sampling time is 2 msec.

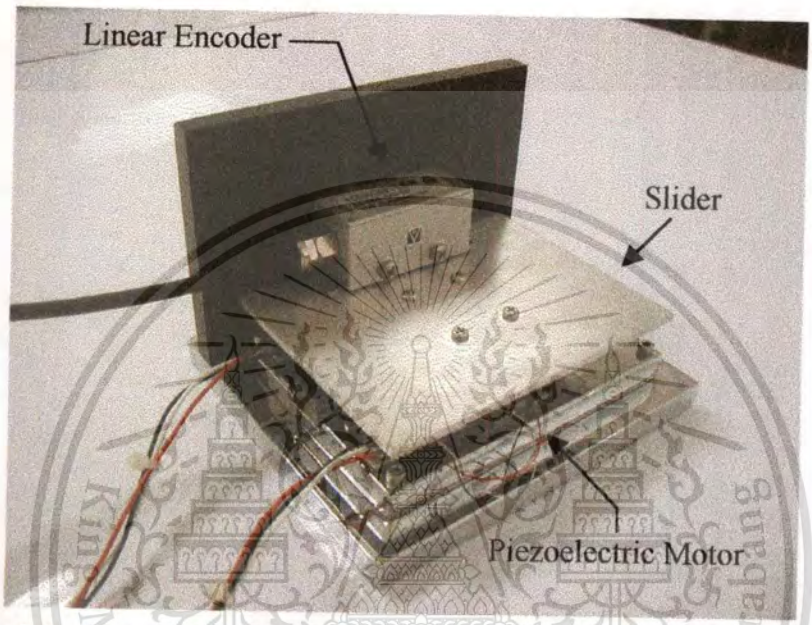

Figure 5.16 Photograph of the ultrasonic linear motor including the linear encoder.

5.4.1 Step Response of Position Control

Figures 5.17 and 5.18 show the experimental results for a 20mm step input with no load mass and its control signal respectively. The response when 0.5kg load mass is placed to the slider is shown in figure 5.19, and its control signal is also shown in figure 5.20. The both response curves have no steady-state error and overshoot, like the response curves obtained from simulation.

Table 5.2 System performance comparison (experiments)

Operating condition	t_r (sec)	P_o (%)	t_s (sec)
No load	0.54	0.00	1.46
Load (0.5kg)	0.57	0.00	1.55

It is found from the table 5.2 that the response speed of no-load condition is slightly different from the response speed of load condition, which demonstrates the robustness. Hence, the

This material is reserved for educational use only, not allowed for commercial use.
Forbidden to modify the content, and cite the document when use.

proposed control system is insensitive to the parameter variations. Therefore, the PDFF controller designed by CDM can assure the desired control performance when the operating condition has been changed.

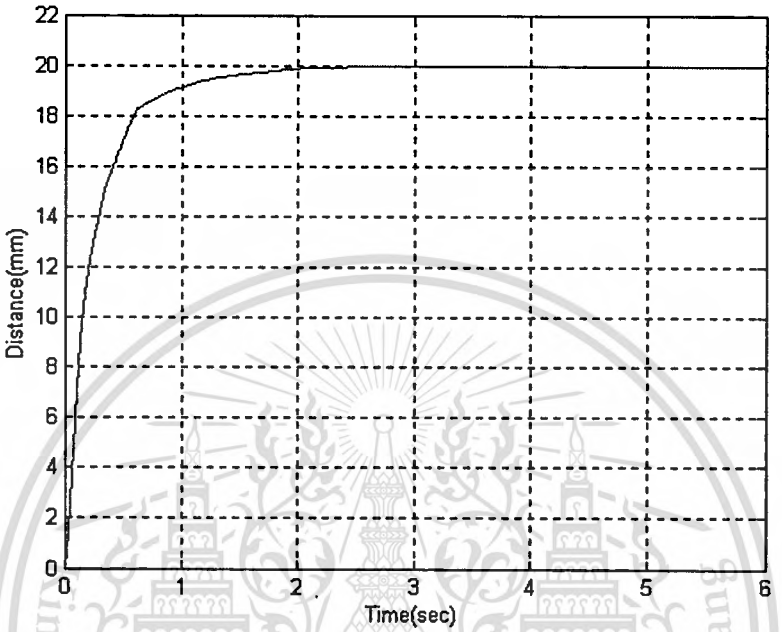

Figure 5.17 Response to step input without load mass.

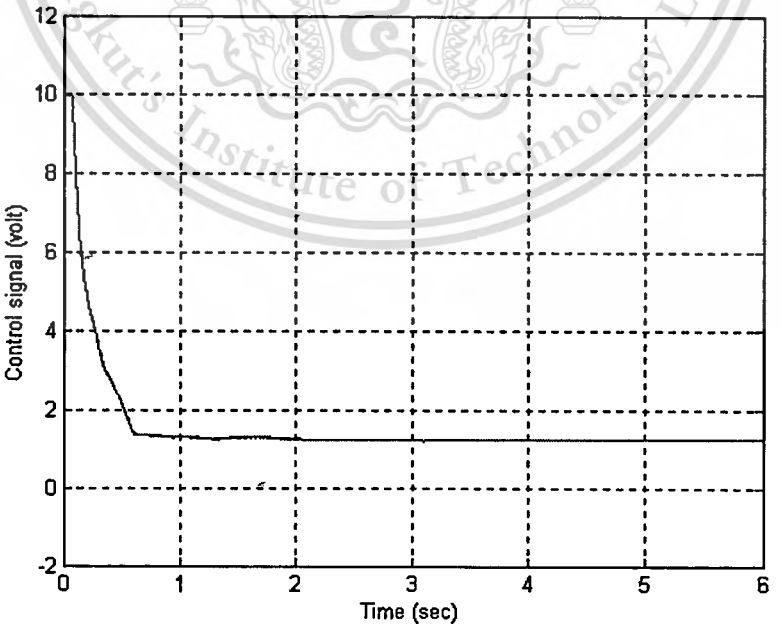

Figure 5.18 Control signal.

This material is reserved for educational use only, not allowed for commercial use.
Forbidden to modify the content, and cite the document when use.

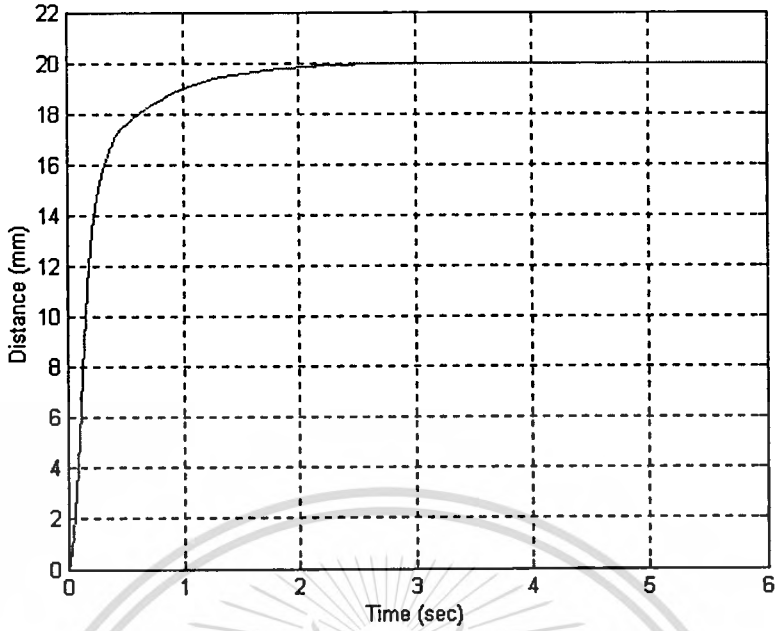

Figure 5.19 Response to step input with 0.5kg load mass.

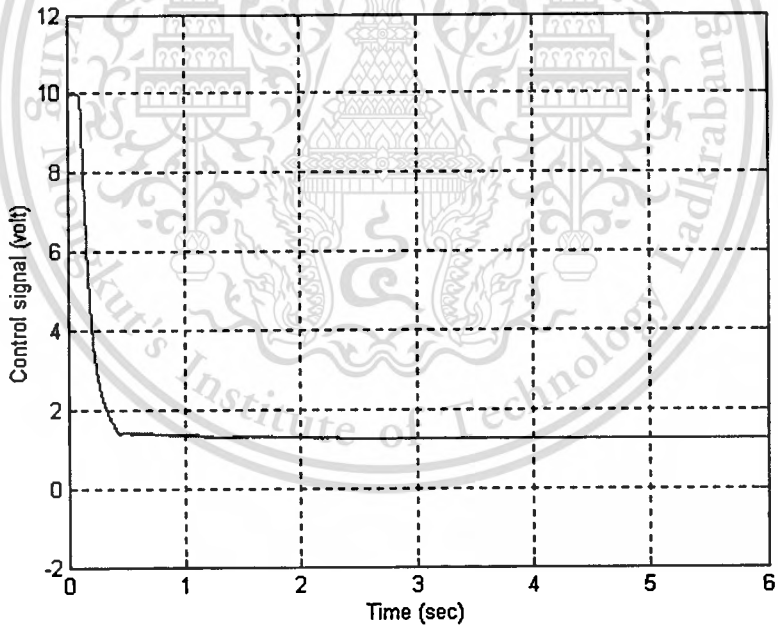

Figure 5.20 Control signal.

5.4.2 Step Response with Constant Disturbance

In this sub-section, the disturbance rejection capability is studied. The response, that a step disturbance equivalent to 1N is applied to the input terminal of ultrasonic linear motor while PDFF control system holds the position at 20mm at 6 seconds, is shown in figure 5.21. Figure 5.22 shows the control signal. It is seen from figure 5.21 that the experiment has similar result to

This material is reserved for educational use only, not allowed for commercial use.
Forbidden to modify the content, and cite the document when use.

the simulation, but the system takes a longer time to eliminate the position error due to the effect of motor driver's deadband.

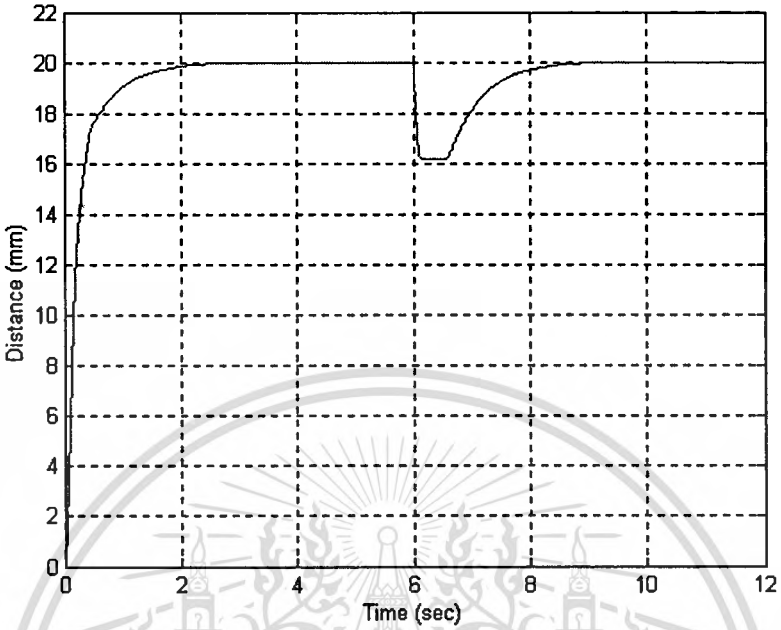

Figure 5.21 Response to step input and step disturbance.

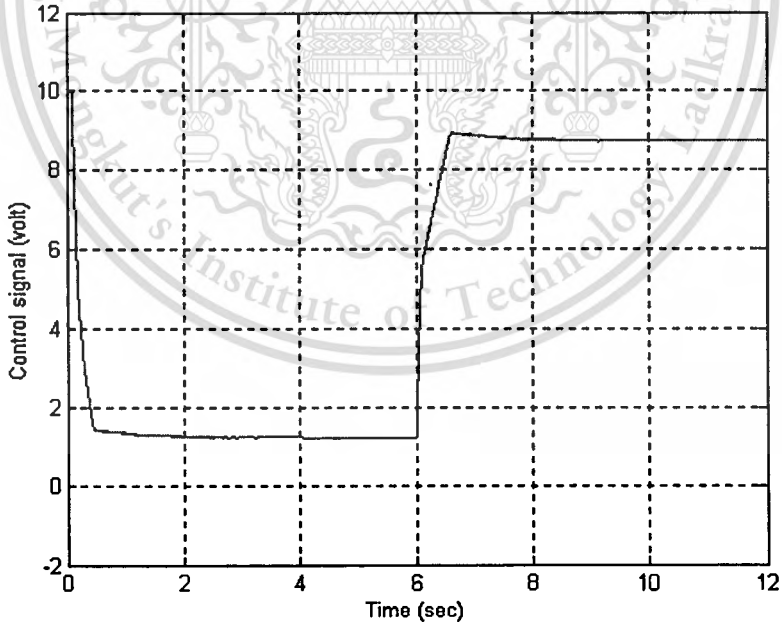

Figure 5.22 Control signal.

5.4.3 Tracking Characteristic

The tracking characteristic of the PDFF position control system is examined by controlling the slider to the positions of 10, 20 and 30mm, of which each time interval is 4 seconds.

This material is reserved for educational use only, not allowed for commercial use.
Forbidden to modify the content, and cite the document when use.

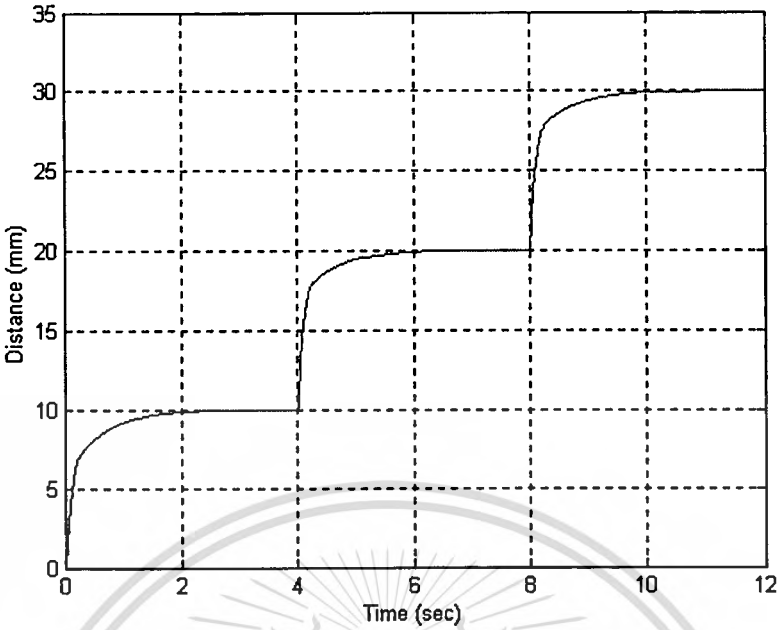

Figure 5.23 Response to stair input without load mass.

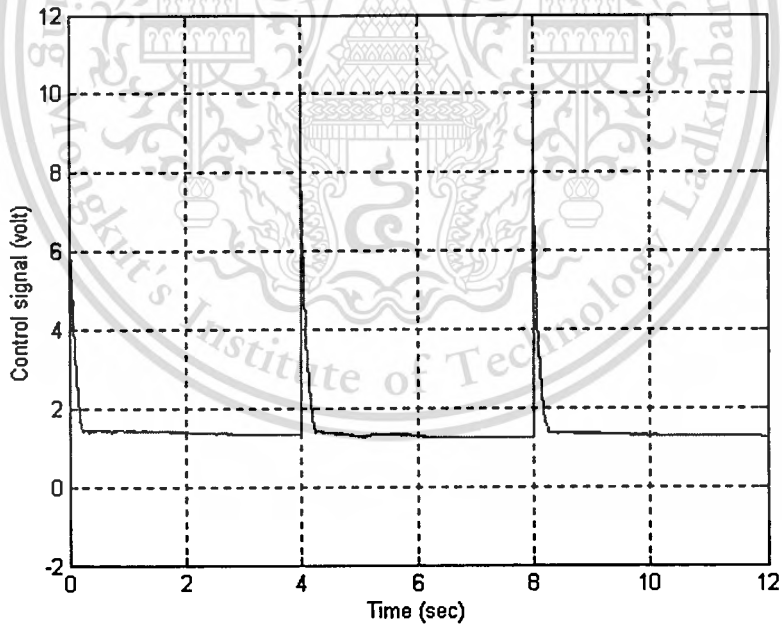

Figure 5.24 Control signal.

Figures 5.23 and 5.24 show the response curve to the stair input for no-load condition and its control signal respectively. There is no steady-state error and overshoot at each time interval (see figure 5.23).

This material is reserved for educational use only, not allowed for commercial use.
Forbidden to modify the content, and cite the document when use.

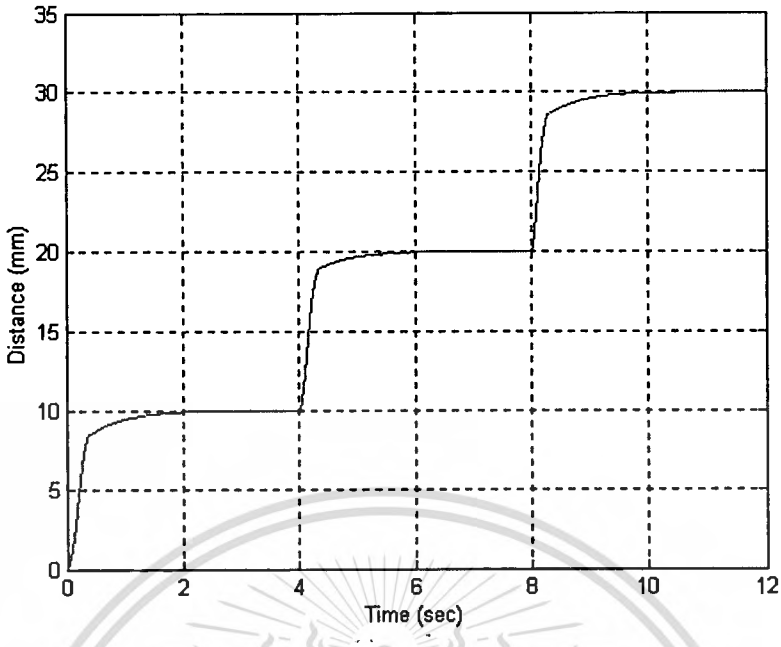

Figure 5.25 Response to stair input with 1kg load mass.

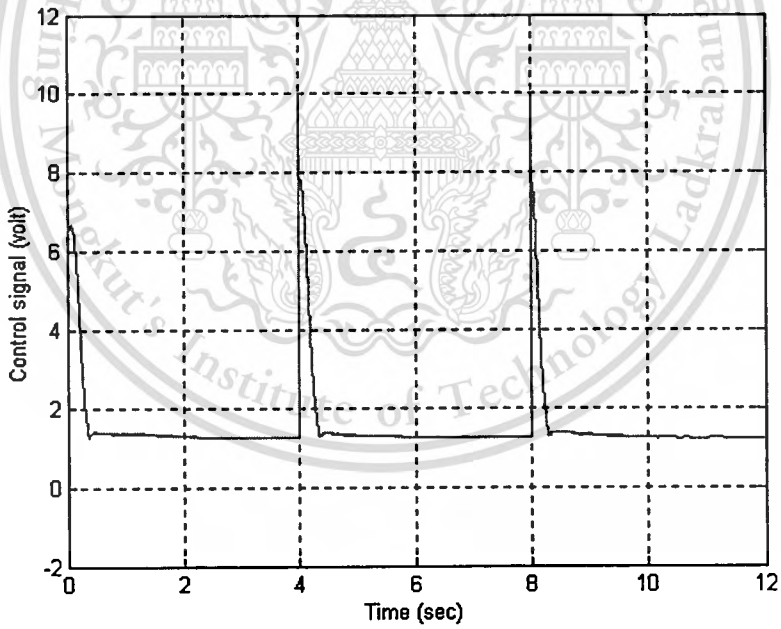

Figure 5.26 Control signal.

When the 1kg load mass is placed on the slider, the response curve remains almost unchanged from the response curve of no-load condition as shown in figure 5.25, and its control signal is also shown in figure 5.26. It can be observed that the fast tracking property and robustness of the proposed position control system can be obtained.

This material is reserved for educational use only, not allowed for commercial use.
Forbidden to modify the content, and cite the document when use.

Chapter 6

Conclusions and Future Works

6.1 Conclusions

The PDFF controller designed by coefficient diagram method has been introduced for controlling the position of ultrasonic linear motor. The reasonable mathematical model of ultrasonic linear motor has been derived so that the CDM can be applied. The transfer function of the PDFF position control in term of γ_i, τ, and α has been developed in general form. Hence, the PDFF controller parameters can be obtained appropriately by assigning the values of γ_i, τ, and α. This form is not only applied to the second-order plant, but also a higher-order plant as well. The simulations and experiments have also been performed. The results indicated that the PDFF control system designed by CDM is robust to the load or parameters changes. Thus, controller parameters need not to be redesigned repeatedly while the control system is operating at the different conditions. Furthermore, the effect of disturbance is small and can be rejected rapidly, and the quick position tracking characteristic can be obtained. In addition, the simulation results of PDFF control system have also been compared with the PD control system. Although, the structure of PD control system is simpler than the structure of PDFF control system, but its result is not satisfied in disturbance rejection capability. Hence, it can be concluded that CDM is successful in the PDFF controller design for quick and precise position control of ultrasonic linear motor.

6.2 Future Works

Ultrasonic linear motors are low cost, compact profile, and suitable for applications requiring manipulation within micrometer range. With these merits, the applications of various types of the ultrasonic linear motors emerge quickly. Future research aims include the following:

- The nonlinear properties of the ultrasonic linear motors, such as heat generation, friction drive, and contact mechanism between driving tip and slider have to be studied to assure the reliability of their operation.

- The deadband of motor driver degrades the regulation performance as presented in sub-section 5.4.2. To overcome this problem, the deadband compensator should be considered.

This material is reserved for educational use only, not allowed for commercial.
Forbidden to modify the content, and cite the document when use.

REFERENCES

[1] Toshiiki Sashida and Takashi Kenjo. **An Introduction to Ultrasonic Motors.** Oxford : Clarendon Press. 1993.

[2] K.K. Tan, Tong Heng Lee, and Huixing X. Zhou. "Micro-Position of Linear-Piezoelectric Motors Based on a Learning Nonlinear PID Controller." IEEE/ASME Transactions on Mechatronics, Vol. 6, No. 4, 2001, pp. 428-436.

[3] Y.Izuno, R.Takeda, and M.Nakaoka. "New Fuzzy Reasoning-Based High-Performance Speed/Position Servo Control Schemes Incorporating Ultrasonic Motor." IEEE Transactions on Industry Applications, Vol. 28, 1992, pp. 613-618.

[4] T.Senjyu, S.Yokoda, and K.Uezato. "Speed Control of Ultrasonic Motors Using Fuzzy Neural Network." IEEE Technical Proceedings of Power Electronics Congress, 1996, pp. 29-34.

[5] S.W.Chung, K.T.Chau, and C.C.Chan. "Neuro-Fuzzy Dual-Mode Control of Travelling-Wave Ultrasonic Motors." IEEE International Conference of Electric Machines and Drives, 1999, pp. 598-600.

[6] T.Senjyu, H.Miyazato, S.Yokoda, and K.Uezato. "Speed Control of Ultrasonic Motors Using Neural Network." IEEE Proceedings of Industrial Electronics, Control, and Instrumentation, 1996, pp. 887-892.

[7] T.Senjyu, H.Miyazato, S.Yokoda, and K.Uezato. "Position Control of Ultrasonic Motors Using Neural Network." IEEE Technical Proceedings of Power Electronics Congress, 1996, pp. 368-373.

[8] T.Senjyu and K.Uezato. "Adjustable Speed Control of Ultrasonic Motors by Adaptive Control." Power Electronics Specialists Conference, Vol. 2, 1994, pp. 1237-1242.

[9] T.Senjyu, H.Miyazato, and K.Uezato. "Quick and Precise Position Control of Ultrasonic Motors Taking Account of Frictional Force Control." IEEE Industry Applications Conference, Vol. 1, 1995, pp. 85-89.

[10] T.Senjyu, H.Miyazato, and K.Uezato. "Quick and Precise Position Control of Ultrasonic Motors with Two Control Inputs." IEEE Power Electronics Specialists Conference, Vol. 1, 1995, pp. 415-420.

This material is reserved for educational use only, not allowed for commercial use.
Forbidden to modify the content, and cite the document when use.

[11] T.Senjyu, H.Miyazato, S.Yokoda, and K.Uezato. "Speed Control of Ultrasonic Motors by Adaptive Control with a Simplified Mathematical Model." IEE Proceedings of Electric Power Applications, Vol. 145, 1998, pp. 180-184.

[12] T.Senjyu, H.Miyazato, S.Yokoda, and K.Uezato. "Performance Comparison of PI and Adaptive Controller for Adjustable Speed Drives of Ultrasonic Motors." IEEE Proceedings of Industrial Technology, 1994, pp. 519-523.

[13] S.Manabe. "Coefficient Diagram Method." 14th IFAC Symposium on Automatic Control in Aerospace, 1998.

[14] D.Y.Ohm. "A PDFF Controller for Tracking and Regulation in Motion Control." Proceedings of 18th PCIM Conference, Intelligent Motion, 1990, pp. 26-36.

[15] D.Isarakorn, S.Panaudomsup, T.Benjanarasuth, J.Ngamwiwit, and N.Komine. "Application of CDM to PDFF Controller for Motion Control System." The 4th Asian Control Conference, 2002, pp. 1173-1177.

[16] D.Isarakorn, S.Panaudomsup, T.Benjanarasuth, J.Ngamwiwit, and N.Komine. "Position Control of Ultrasonic Linear Motor using PDFF Controller Designed by CDM." International Symposium on Nonlinear Theory and its Applications, 2002, pp. 897-900.

[17] S.Furuya, T.Marushi, and M.Nakaoka. "A Compact Ultrasonic Motor-actuated Software System Implementation using Fuzzy Reasoning-based Controller." Fifth International Conference on Electrical Machines and Drives, 1991, pp. 232-236.

[18] T.Senjyu, H.Miyazato, S.Yokoda, and K.Uezato. "A Study on High Efficiency Drive of Ultrasonic Motors." IEEE Proceedings of Power Electronics and Drive Systems, 1997, pp. 365-370.

[19] A.Lipatov and N.Sokolov. "Some Sufficient Conditions for Stability and Instability of Continuous Linear Stationary Systems." Automat. Remote Cont., 1979, pp. 1285-1291.

[20] D.Kumpanya, T.Benjanarasuth, J.Ngamwiwit, and N.Komine. "PI Controller Design with Feedforward by CDM for Level Process." TENCON2000, Vol. 2, 2000, pp. 65-69.

[21] EDO Electro-Ceramic Products. "High Speed Piezoelectric Micropositioning Motor." U.S. Patent no. 4622483, March 2001.

This material is reserved for educational use only, not allowed for commercial use.
Forbidden to modify the content, and cite the document when use.

Appendix A

Equivalent-circuit Analysis for Piezoelectric Ceramic

The piezoelectric ceramics are the most important elements of the ultrasonic linear motor. In order to understand how these elements applied in the ultrasonic linear motor, the equivalent circuit must be developed. This equivalent circuit is used to regard the electrical-to-mechanical energy transformation.

A.1 Piezoelectric Equations

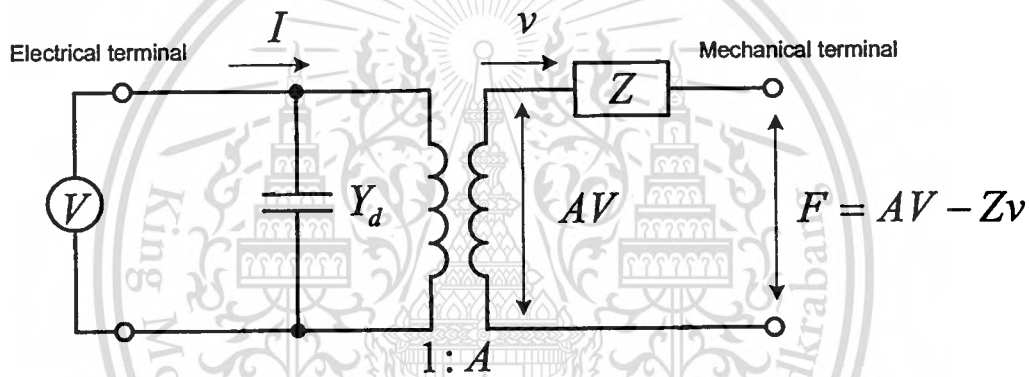

Figure A.1 An electromechanical transducer circuit.

In describing the behavior of the systems that employ piezoelectric ceramics, the following equations are important:

$$F = AV - Zv \tag{A.1}$$

$$I = Y_d V + Av \tag{A.2}$$

where F is the force at the mechanical terminals, A is a force factor which is employed in electroacoustic transducer theory, v is the velocity at the mechanical terminals, V is the voltage at the electrical terminals, I is the current at the electrical terminals, Z is the mechanical impedance of the ceramic material and Y_d is the blocking admittance.

This material is reserved for educational use only, not allowed for commercial use.
Forbidden to modify the content, and cite the document when use.

To illustrate these equations, an equivalent circuit is shown in figure A.1. In equation (A.1), the first term on the right-hand side is the force generated within the ceramic body, which is equal to the applied voltage V multiplied by A. If this force AV is subtracted by the impedance drop, which is the product of the internal mechanical impedance Z and velocity v, the result is the force exerted by the motor externally. Thus the force factor A is the force created when a unit voltage is applied.

Consider equation (A.2). $Y_d V$ is the current flowing through the capacitance and Av is the current which causes the ceramic body to deform. Thus the force factor A is the current generated when unit velocity is given to the ceramic body. In general, the unit of A depends on the properties and dimensions of the ceramic and how it is used.

The electromechanical transducer circuit can be simplified by incorporating the transformer element into the internal impedance Z. The result, with a modified internal impedance Z_m, is shown in figure A.2.

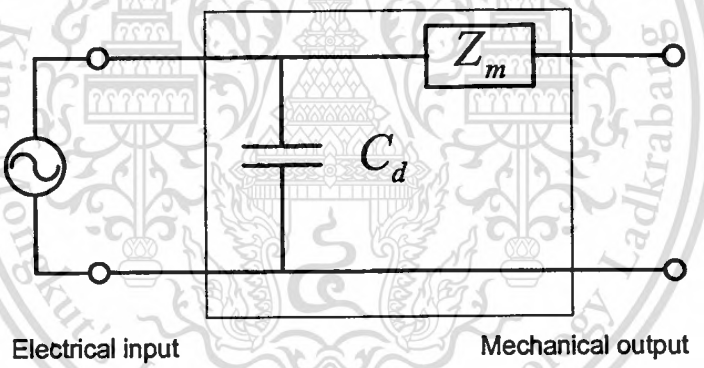

Figure A.2 Simplified circuit for figure A.1.

A.2 Internal Impedance

The internal impedance Z_m in figure A.2 will be examined to show that this circuit is a resonant circuit. When DC voltage is applied with no mechanical load, the piezoelectric ceramic will reach equilibrium after undergoing an initial deformation. This is analogous to a spring under a constant force, which can be expressed by

$$F = Kx, \tag{A.3}$$

where F is the applied force, x is the displacement and K is the spring constant.

This material is reserved for educational use only, not allowed for commercial use.
Forbidden to modify the content, and cite the document when use.

The current created, when unit velocity is given can be expressed by

$$I = Av. \tag{A.4}$$

Integrating both sides with respect to time, it is the charge q created by a unit displacement x. Thus

$$q = Ax. \tag{A.5}$$

The force generated in a piezoelectric ceramic is

$$F = AV. \tag{A.6}$$

Substituting equations (A.5) and (A.6) into equation (A.3), we obtain

$$AV = \frac{q}{A}K \tag{A.7}$$

or

$$V = \frac{K}{A^2}q. \tag{A.8}$$

The equivalent capacitance is then given by

$$C = \frac{A^2}{K}. \tag{A.9}$$

Consider now the forced vibrations of a piezoelectric ceramic when an AC voltage is applied. If ceramic is bonded to metal, the metal will also vibrate. A model describing this behavior is shown in figure A.3, where (b) shows the forced vibration of the mass-spring system under a force f, generated by the AC voltage V.

This material is reserved for educational use only, not allowed for commercial use.
Forbidden to modify the content, and cite the document when use.

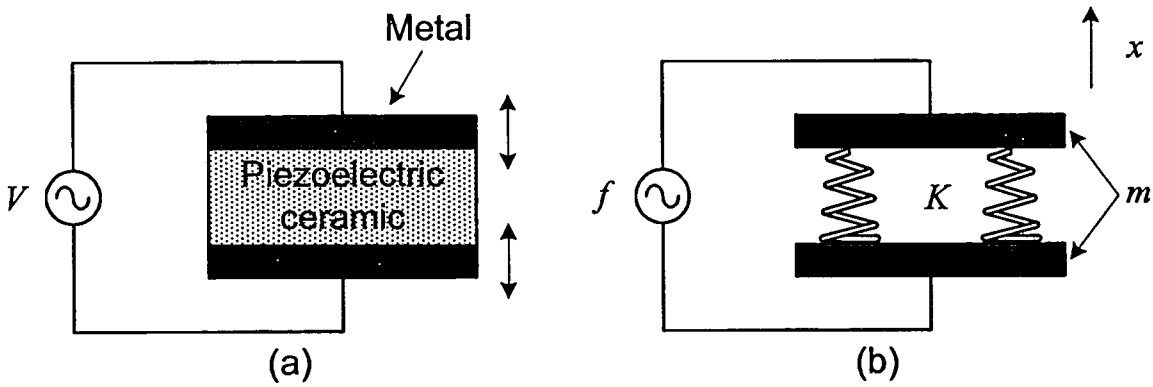

Figure A.3 AC voltage applied to a combined piezoelectric-ceramic-metal element and a mechanically equivalent model: (a) electrical-mechanical transformation and (b) mechanical model.

In figure A.3, the equation of motion is given by

$$m\frac{d^2x}{dt^2}+Kx=f(x), \tag{A.10}$$

where m is a mass of the piezoelectric-ceramic-metal element. If equation (A.5) is substituted into this equation and express it in terms of q, then divide both sides by A, we obtain

$$\frac{m}{A^2}\frac{d^2q}{dt^2}+\frac{K}{A^2}q=\frac{f(x)}{A}. \tag{A.11}$$

From equation (A.6), the term on the right-hand side is the applied voltage. On the other hand, the equivalent capacitance C, equivalent inductance L, and voltage $V(t)$ are related by

$$L\frac{d^2q}{dt^2}+\frac{1}{C}q=V. \tag{A.12}$$

The second derivative in equations (A.11) and (A.12) must be equal, the equivalent inductance is then given by

$$L=\frac{m}{A^2}. \tag{A.13}$$

This material is reserved for educational use only, not allowed for commercial use.
Forbidden to modify the content, and cite the document when use.

To construct an equivalent circuit, the mass m is represented by the inductance L and place it in series with capacitor C. This is shown in figure A.4.

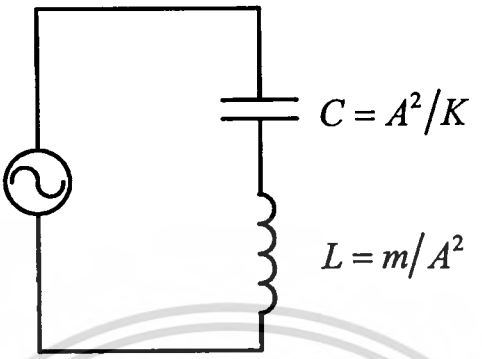

Figure A.4 Equivalent circuit for the model in figure A.3.

A.3 Basic Equivalent Circuit

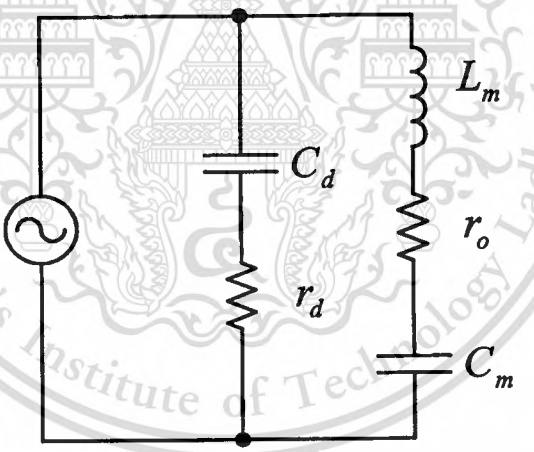

Figure A.5 Equivalent circuit with elements representing losses.

By improving the equivalent circuit in the previous sub-section, the circuit shown in figure A.5 can be obtained. This circuit represents free vibrations of a stator with no loads, and includes two resistors which represent losses. The elements that have been added are given below.

This material is reserved for educational use only, not allowed for commercial use.
Forbidden to modify the content, and cite the document when use.

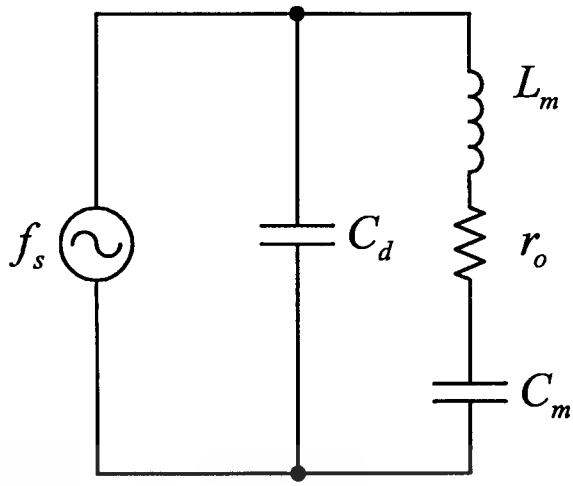

Figure A.6 Basic equivalent circuit.

C_d: This is a capacitance due to the element's dielectric properties, called the 'blocking capacitance'. It is the capacitance measured when the ceramic element is fixed so that no vibrations can occur. In this condition, there is no motion in the system.

r_d: This resistance represents the dielectric loss. When an AC voltage is applied to a regular dielectric, hysteresis is created between the electric field E and the electric flux density D, and heat is generated. This loss can be ignored at higher frequencies. The combination of C_d and r_d in the form $\left(r_d + 1/j\omega C_d\right)$ is called the blocking impedance. Since r_d can be neglected for the frequency range of the ultrasonic linear motor, it will be omitted in subsequent circuit (see figure A.6).

r_o: This resistance is called the 'internal resistance', which represents the various mechanical losses occur in components such as the vibrator's metal block, the bonded surfaces of the piezoelectric ceramics, and stator and electrodes. When r_o, C_m and L_m are combined in the form $\left(r_o + j\omega L_m + 1/j\omega C_m\right)$, this is known as the motional impedance.

This material is reserved for educational use only, not allowed for commercial use.
Forbidden to modify the content, and cite the document when use.

Appendix B

Effect of Tuning Factor

The tuning factor α effects directly to the response speed. Normally, a faster response can be obtained from a larger value of tuning factor α. However, the fast response may lead to high overshoot. Hence, the effect of tuning factor α to response speed should be studied in order to find its satisfied value that gives a fast response without overshoot. This study will be done on numerical examples via simulation.

The response curves of the system shown in figure 4.2 to the unit-step input with various values of α are now determined into the standard stability index value case and the larger stability index value case.

(1) Standard stability index value case ($\gamma_1 = 2.5$ and $\gamma_2 = 2$): The unit-step response curves for $\tau = 0.5$ and $\tau = 5$ are shown in figures B.1 and B.2 respectively.

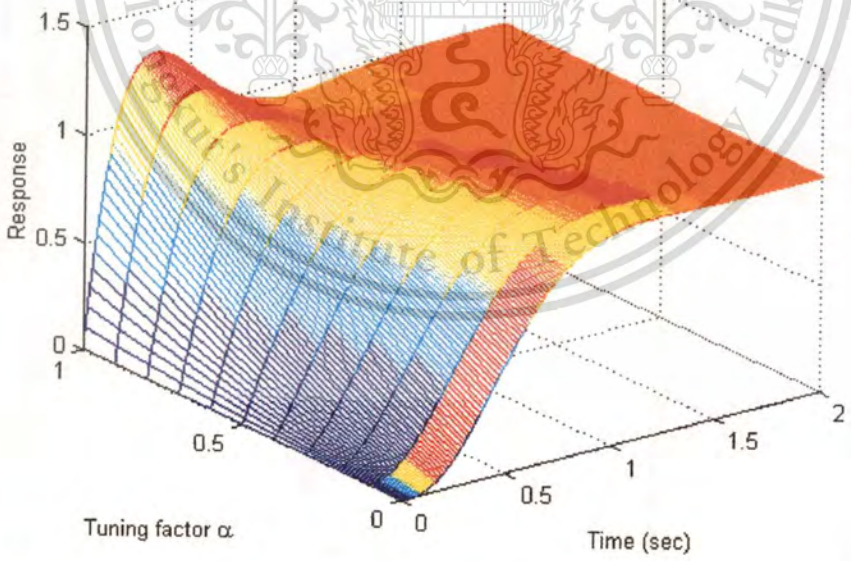

Figure B.1 Unit-step response curves for $\gamma_1 = 2.5$, $\gamma_2 = 2$ and $\tau = 0.5$.

This material is reserved for educational use only, not allowed for commercial use.
Forbidden to modify the content, and cite the document when use.

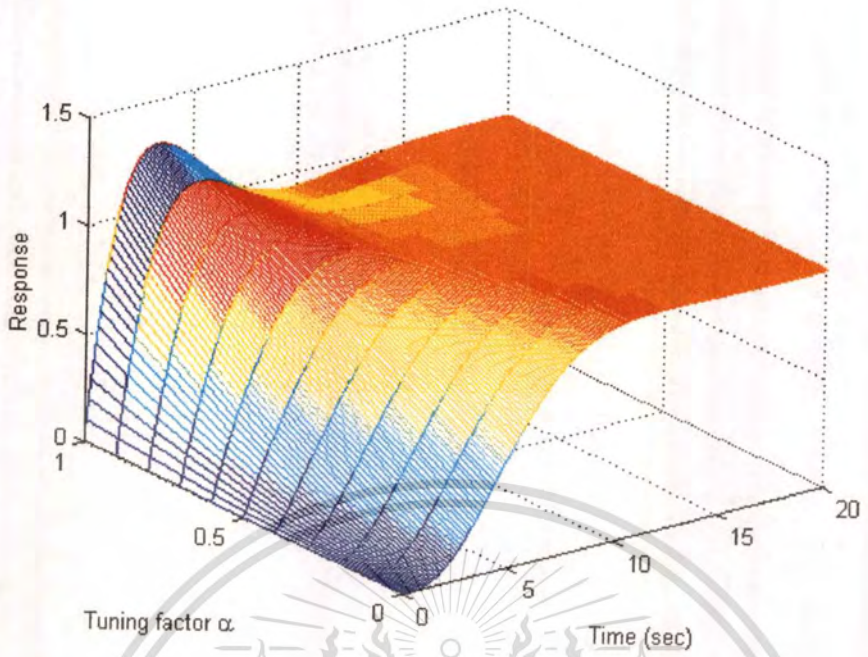

Figure B.2 Unit-step response curves for $\gamma_1 = 2.5$, $\gamma_2 = 2$ and $\tau = 5$.

(2) Larger stability index value case: The unit-step response curves for $\gamma_1 = 5$ and $\gamma_2 = 4$, and for $\gamma_1 = 7.5$ and $\gamma_2 = 6$ with the same $\tau = 0.5$ are shown in figures B.3 and B.4 respectively.

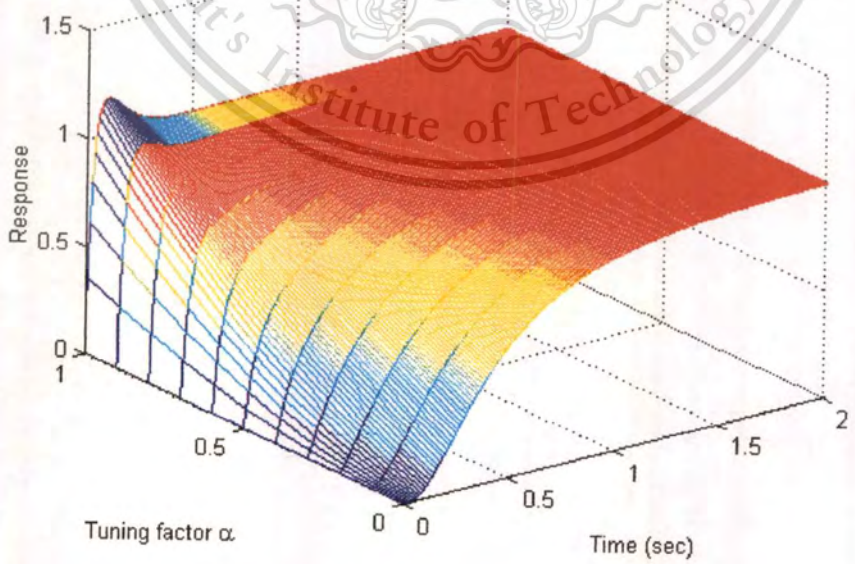

Figure B.3 Unit-step response curves for $\gamma_1 = 5$, $\gamma_2 = 4$ and $\tau = 0.5$.

This material is reserved for educational use only, not allowed for commercial use.
Forbidden to modify the content, and cite the document when use.

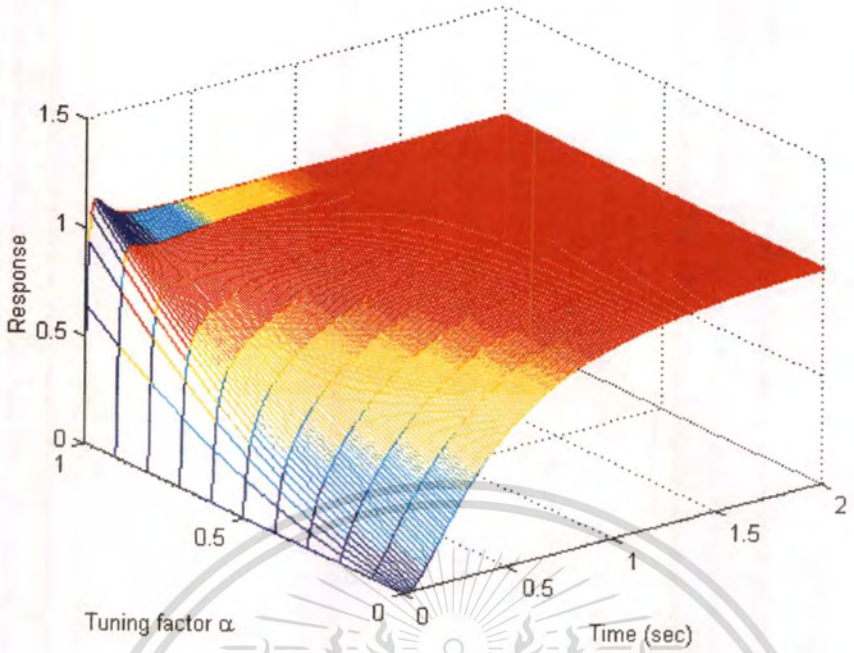

Figure B.4 Unit-step response curves for $\gamma_1 = 7.5$, $\gamma_2 = 6$ and $\tau = 0.5$.

From figures B.1 and B.2, the fastest responses without overshoot can be obtained from $\alpha = 0.6$ even though the equivalent time constants τ are different. In case of larger stability index value $\alpha = 0.8$ and $\alpha = 0.9$ that give the fastest responses with no overshoot are shown in figure B.3 and figure B.4 respectively. In this case, although, the large value of α can be selected but it is obvious that the response curves are not quite smooth. The satisfied value of α should be around 0.6 to 0.8.

In actual design, the choice of the standard stability index is strongly recommended. Thus, the initial selection of α should be 0.6. Sometimes a designer may select the larger value of α, if the value of stability index is large.

This material is reserved for educational use only, not allowed for commercial use.
Forbidden to modify the content, and cite the document when use.

Appendix C

Related Publication

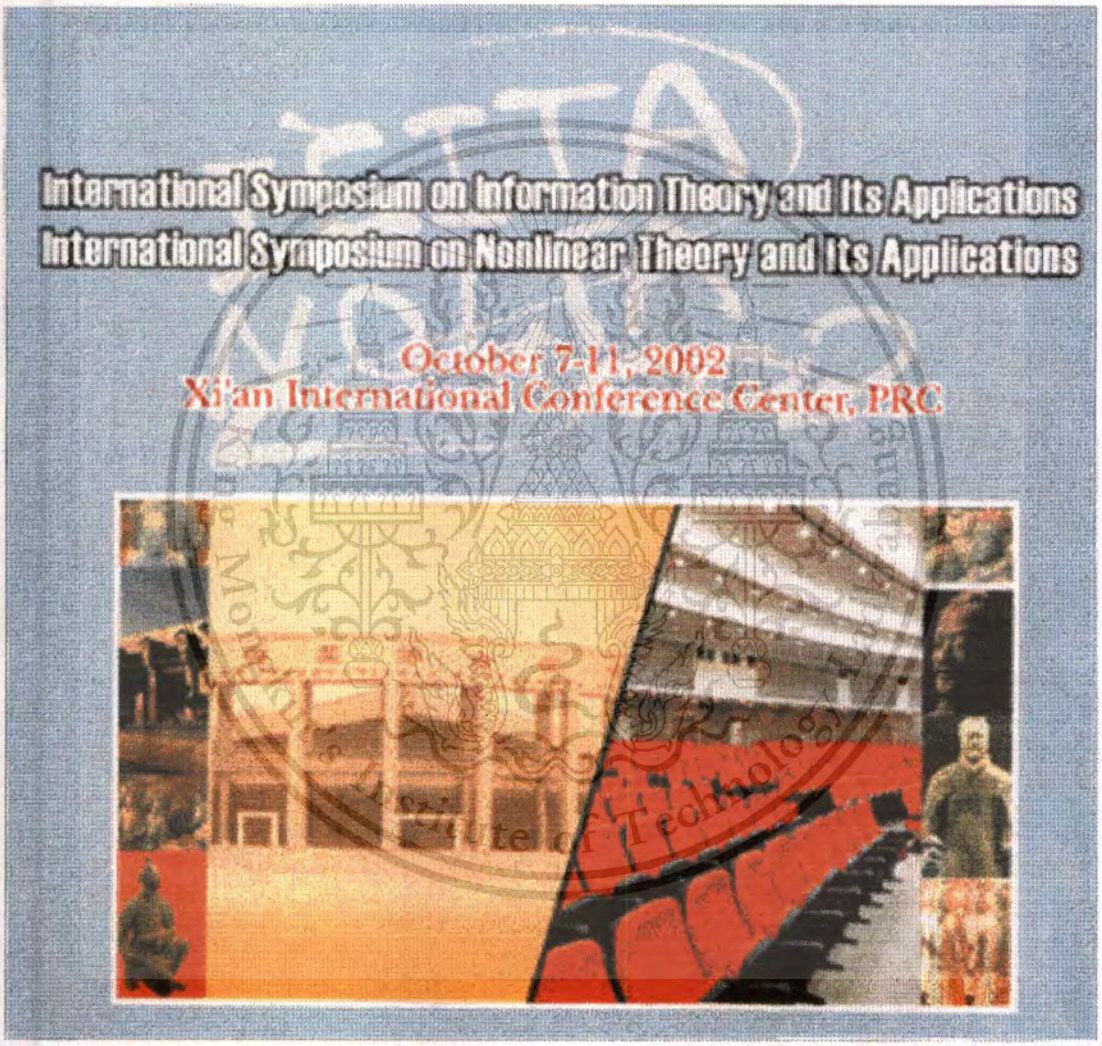

This material is reserved for educational use only, not allowed for commercial use.
Forbidden to modify the content, and cite the document when use.

International Symposium on Nonlinear Theory and its Applications
Xi'an, PRC, October 7-11, 2002

Position Control of Ultrasonic Linear Motor using PDFF Controller Designed by CDM

.D. Isarakorn*, S. Panaudomsup*, T. Benjanarasuth*, J. Ngamwiwit* and N. Komine**

*Department of Control Engineering,
Faculty of Engineering and Research Center for Communications and Information Technology
King Mongkut's Institute of Technology Ladkrabang, Ladkrabang, Bangkok, 10520 Thailand
Tel: 66-2-326-4221, Fax: 66-2-326-4221, E-mail: knjongko@kmitl.ac.th
**Department of Applied Computer Engineering,
School of Information Technology and Electronics, Tokai University
1117 Kitakaname, Hiratsuka-Shi, Kanagawa-Ken, 259-1292, Japan
Tel: 81-463-58-1211, Fax: 81-463-50-2240, E-mail: komine@keyaki.cc.u-tokai.ac.jp

Abstract: This paper presents a new position control scheme of ultrasonic linear motor using PDFF controller (Pseudo-Derivative Control with Feedforward Gains) designed by CDM (Coefficient Diagram Method). The PDFF controller satisfies the tracking, regulation, and robustness. The effectiveness of the proposed controller is demonstrated by the simulation and the experimental results.

I. Introduction

The ultrasonic linear motor is a type of indirect-drive piezoelectric motor which uses piezoelectric ceramic crystals to generate waves with a frequency in the ultrasonic range and produces a linear motion [1]. The advantages of ultrasonic motor are high precision, quick response, hard brake with no backlash, high power to weight ratio and negligible EMI. However, the mathematical model of the ultrasonic motor is complex to apply for position control.

In recent years, many control schemes have been proposed to control the position of ultrasonic motors, such as fuzzy logic control, adaptive control and neural network control. Fuzzy logic control is a simple technique to control a complex system because it does not need to use a mathematical model [2]. Nevertheless, extract of fuzzy rules depends on experience and intuition of the designer, and its tuning is tedious duties. Adaptive control algorithm has been used to maintain good performance of the servo system subjected to torque disturbance and parameter variations [3]. However, adaptive control techniques have many difficulties when apply to actual implement. Neural network has a good potential for control applications because it can approximate the nonlinear input-output mappings of the plant, but there is some error while the network is learning [4].

This paper presents a position control of ultrasonic linear motor using PDFF controller designed by CDM [5]. The parameters of the PDFF controller are designed based on the stability and the speed of the controlled system. Stability and speed are designed from the standard stability index γ_i and the equivalent time constant τ respectively. The stability index γ_i and the equivalent time constant τ are defined based on the coefficients of the characteristic polynomial of the closed-loop transfer function. These coefficients are related to the controller parameters algebraically in an explicit form. According to the design methodology of the CDM, the parameters of the PDFF controller can be obtained easily.

2. Modeling of Ultrasonic Linear Motor

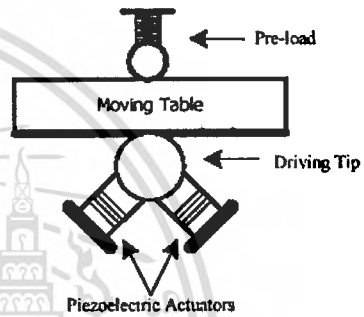

Fig. 1. Structure of an ultrasonic linear motor.

The principal structure of an ultrasonic linear motor considered in this work is shown in Fig. 1. The stator is fitted with two piezoelectric stack actuators positioned orthogonal to each other. They are driven by two electrical sources of identical frequency, but with a phase difference. Thus, an elliptical motion is created at the driving tip. It is coupled to the moving table. Each vibration cycle is transformed to linear motion by friction force. The friction force serves as the driving force for the moving table. Therefore, the ultrasonic linear motor is then a high nonlinear system and must be modeled to be a linear system so that CDM can be applied. In this paper, the ultrasonic linear motor is modeled as a second-order differential equation [1]

$$m\ddot{x} = k_f v - b\dot{x} \tag{1}$$

where m, x, b, v and k_f denote the total moving mass, the position, the viscous damping coefficient, the control input voltage, and the thrust force constant respectively. Hence, the ultrasonic linear motor transfer function is

$$G_p(s) = \frac{X(s)}{V(s)} = \frac{k_f}{s(ms+b)}. \tag{2}$$

3. Control System Structure

The general structure of PDFF control system consisting of feedforward controller, feedback controller, integral controller and plant is shown in Fig. 2. K_{ff} and K_{fp}, K_p and K_d are the proportional gain and derivative gain of the feedforward and of the feedback controllers, respectively.

This material is reserved for educational use only, not allowed for commercial use.

Forbidden to modify the content, and cite the document when use.

and K_i is the integral gain of the integral controller. $D(s)$ is the disturbance. The transfer function from $R(s)$ to $C(s)$ is given as

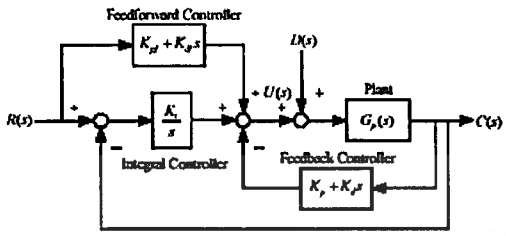

Fig. 2. Structure of PDFF control system.

$$\frac{C(s)}{R(s)}=\frac{G_p(s)\left[K_{ff}+\frac{K_i}{s}+K_{df}s\right]}{1+G_p(s)\left[K_p+\frac{K_i}{s}+K_d s\right]} \tag{3}$$

In order to use CDM to design the controller gains properly, the controlled system consisting of the CDM standard block diagram of SISO system with the feedforward and feedback controllers is proposed. $A_p(s)$ and $B_p(s)$ are the polynomials of the plant $G_p(s)$, $A_c(s)$, $B_c(s)$ and $B_a(s)$ are the polynomials of the CDM controller, $B_g(s)$ is the polynomial of the feedforward controller and $B_{fb}(s)$ is the polynomial of the feedback controller. After rearranging the plant and the feedback controller shown in Fig. 3, $A_p^*(s)$ and $B_p^*(s)$ which are the polynomials of the modified plant $G_p^*(s)$ can be obtained and is shown in Fig.4.

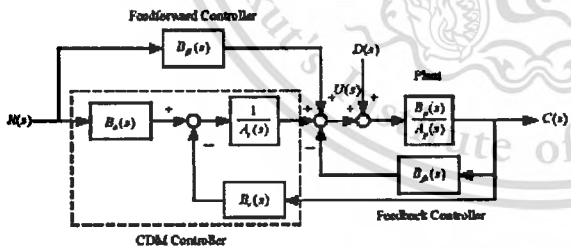

Fig. 3. CDM standard block diagram of SISO system with the feedforward controller.

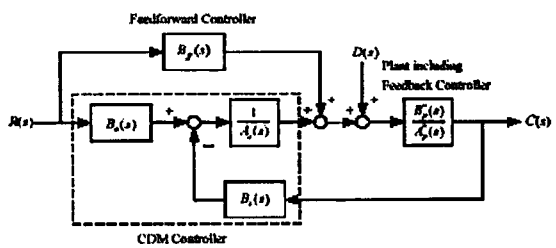

Fig. 4. Rearranged CDM standard block diagram.

From the block diagram of Fig. 4 it follows:

$$\frac{C(s)}{R(s)}=\frac{B_p^*(s)[B_a(s)+B_g(s)A_c(s)]}{A_c(s)A_p^*(s)+B_c(s)B_p^*(s)} \tag{4}$$

and

$$\frac{C(s)}{D(s)}=\frac{A_c(s)B_p^*(s)}{A_c(s)A_p^*(s)+B_c(s)B_p^*(s)}. \tag{5}$$

It is seen from (4) and (5) that the feedforward controller $B_g(s)$ has an influence on the transfer function from $R(s)$ to $C(s)$ and can be used to increase the speed of the transient response of the controlled system, while the transfer function from $D(s)$ to $C(s)$ is not affected.

4. Coefficient Diagram Method

The CDM is an algebraic control design approach. Polynomials are used for system representation. CDM design is based on a stability index γ_i and an equivalent time constant τ as defined later.

From Fig. 4, the transfer function of the modified plant $G_p^*(s)$ in the polynomial forms can be expressed as

$$A_p^*(s)=p_k s^k+p_{k-1}s^{k-1}+\ldots+p_0 \tag{6a}$$

$$B_p^*(s)=q_m s^m+q_{m-1}s^{m-1}+\ldots+q_0 \tag{6b}$$

and the controller in the polynomial forms are given by

$$A_c(s)=l_\lambda s^\lambda+l_{\lambda-1}s^{\lambda-1}+\ldots+l_0 \tag{7a}$$

$$B_c(s)=k_\lambda s^\lambda+k_{\lambda-1}s^{\lambda-1}+\ldots+k_0 \tag{7b}$$

$$B_a(s)=k_0 \tag{7c}$$

where $\lambda<k$ and $m<k$. $B_a(s)$ is a pre-filter and is to be k_0 in order to obtain the step response with zero steady-state error. Hence, the characteristic polynomial of the closed-loop system without feedforward controller is

$$P(s)=A_c(s)A_p^*(s)+B_c(s)B_p^*(s)=\sum_{i=0}^{n}a_i s^i \tag{8}$$

where $a_0, a_1, \ldots, a_n$ are the coefficients of the characteristic polynomial. The stability index γ_i, the equivalent time constant τ and stability limit γ_i^* are defined as follows:

$$\gamma_i=\frac{a_i^2}{a_{i+1}a_{i-1}} \tag{9}$$

$$\tau=\frac{a_1}{a_0} \tag{10}$$

$$\gamma_i^*=\frac{1}{\gamma_{i+1}}+\frac{1}{\gamma_{i-1}}\ ;\quad \gamma_0,\gamma_n=\infty \tag{11}$$

where $i=1,\ldots,n-1$. In general, the equivalent time constant τ and the standard stability index γ_i are chosen as follows:

$$\tau=\frac{l_1}{2.5}=\frac{l_0}{3} \tag{12}$$

$$\gamma_i=[2.5,2,2,\ldots,2]\ ;\quad i=1,\ldots,n-1 \tag{13}$$

This material is reserved for educational use only, not allowed for commercial use.
Forbidden to modify the content, and cite the document when use.

where t_s is the user specified settling time. In the actual design, the stability index $\gamma_1 = 2.5, \gamma_2 = \gamma_3 = 2$ are strongly recommended. However, for $\gamma_{n-1} - \gamma_4^*$, the condition can be relaxed as

$$\gamma_i > 1.5\gamma_i^*, \quad n-1 \geq i \geq 4. \tag{14}$$

The standard values stated in (13) can be used to design the controller if the following condition is satisfied

$$p_k / p_{k-1} > \tau f(\gamma_{n-1}, \gamma_{n-2} \cdots \gamma_1), \tag{15}$$

where p_k and p_{k-1} are the coefficients of the plant at k^{th} and $(k-1)^{th}$. If the above condition is not met, γ_{n-1} is first increased then γ_{n-2} and so on, until (15) is satisfied. From (9) to (11), the coefficient a_i can be written by

$$a_i = a_0 \tau^i \frac{1}{\gamma_{i-1}\gamma_{i-2}^2 \cdots \gamma_2^{i-2}\gamma_1^{i-1}}. \tag{16}$$

Then the characteristic polynomial will be expressed in term of a_0, τ and γ_i as

$$P(s) = a_0 \left[\left\{ \sum_{i=2}^{n} \left(\prod_{j=1}^{i-1} \frac{1}{\gamma_{i-j}^j} \right) (\tau s)^i \right\} + \tau s + 1 \right]. \tag{17}$$

5. Controller Design

From the concept of CDM stated in section 4, the transfer function $C(s)/R(s)$ of the PDFF control system for the plant $G_p(s)$ shown in (2) is first obtained as

$$\frac{C(s)}{R(s)} = \frac{\frac{(\alpha\tau)^2}{\gamma_1} s^2 + (\alpha\tau)s + 1}{\frac{\tau^3}{\gamma_1^2\gamma_2} s^3 + \frac{\tau^2}{\gamma_1} s^2 + \tau s + 1}, \tag{18}$$

where α is the tuning factor and defined as $0 < \alpha \leq 1$.

In order to assign the proper controller gains of the feedforward controller, feedback controller and integral controller, the transfer function (4) is found from the modified plant

$$G_p^*(s) = \frac{B_p^*(s)}{A_p^*(s)} = \frac{B_p(s)}{A_p(s) + \left[(k_1 + k_2 s) B_p(s) \right]}, \tag{19}$$

the integral controller

$$G_c(s) = \frac{B_c(s)}{A_c(s)} = \frac{k_0}{s}, \tag{20}$$

the feedforward controller

$$B_{ff} = m_1 s + m_0, \tag{21}$$

and the pre-filter

$$B_a(s) = k_0, \tag{22}$$

where $k_2 = K_d$, $k_1 = K_p$, $k_0 = K_i$, $m_1 = K_{ff}$ and $m_0 = K_{ff}$. Then equates it to (18).

6. Simulation and Experimental Results

The simulation and implement are carried on a single axis linear stage driven by two piezoelectric motors model PDA130 as shown in Fig. 5. The linear encoder detects the actual position of the table with the resolution of 20 μm. The maximum stroke of the moving table is about 30 mm.

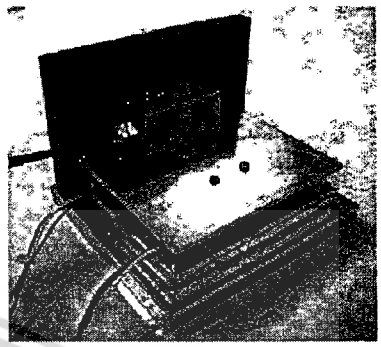

Fig. 5. Photograph of the single axis linear stage.

The gains of the PDFF controller have to be assigned for simulation and implementation. Hence, the parameters of the model are first determined from experimental data based on the technique described in [6], and the model of the single axis linear stage becomes

$$G_p(s) = \frac{0.23}{s(0.12s + 19.88)}.$$

Next, the controller gains are designed by setting the stability indices $\gamma_1 = 7$ and $\gamma_2 = 15$, the equivalent time constant $\tau = 0.4$ second, for $t_s = 1$ second, and the tuning factor α is 0.6 [7]. Thus, the gains of the PDFF controller obtained from the design procedure stated in section 5 are $K_p = 2383.95$, $K_i = 5959.87$, $K_d = 49.80$, $K_{ff} = 1430.37$ and $K_{ff} = 49.04$, respectively.

6.1. Simulation Results

The simulations of the PDFF control system shown in Fig. 2 for a 10mm step input with 0.1kg load mass on the table and a 1N step disturbance applied at 3 seconds are shown in Fig. 6. It is seen that this response exhibits a rise time of 0.40 second without overshoot, and a settling time of 0.95 second. The steady-state error is zero.

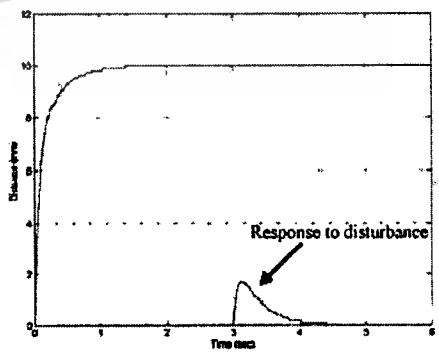

Fig. 6. Responses for a 10mm step input and a 1N step disturbance with 0.1kg load mass.

This material is reserved for educational use only, not allowed for commercial use.
Forbidden to modify the content, and cite the document when use.

In order to demonstrate the effectiveness of the PDFF controller, the 1kg load mass is added on the table without changing the controller gains. The system response for the same 10mm step input and the 1N step disturbance can be shown in Fig. 7. The response has the rise time and the settling time of 0.40 second and 0.97 second. There is no overshoot.

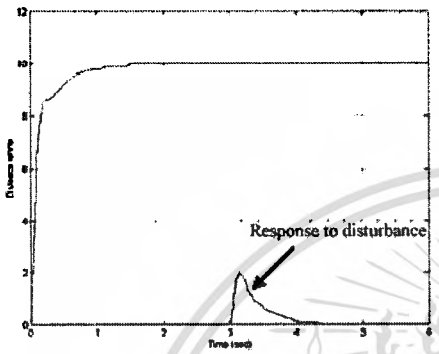

Fig. 7. Responses for a 10mm step input and a 1N step disturbance with 1kg load mass.

It can be summarized that the two position responses are almost identical. Futhermore, the PDFF control systems can rapidly correct the position error caused by the disturbance.

6.2. Experimental Results

The PDFF controller is implemented to control the position of ultrasonic linear motor. The experimental results for a 10mm step input with load mass of 0.1kg and 1kg are shown in Fig. 8 and Fig. 9 respectively.

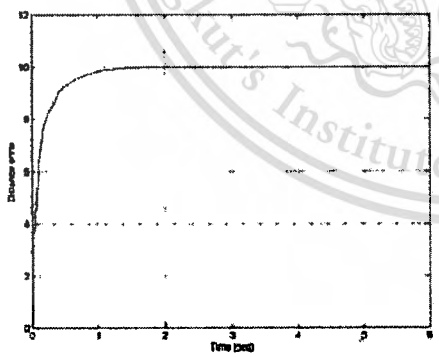

Fig. 8. Experimental result of a 10mm step response for 0.1kg load mass.

The response of Fig. 8 exhibits the rise time of 0.39 second without overshoot, and the settling time of 0.95 second. Figure 9 shows the response when 1kg load mass is added to the table. The rise time and the settling time of the PDFF control system are 0.29 second and 0.85 second, respectively, and there is no overshoot.

From simulation and experimental results, it is observed that the tracking performance, regulation, and robustness for the position control system of the proposed control scheme can be obtained.

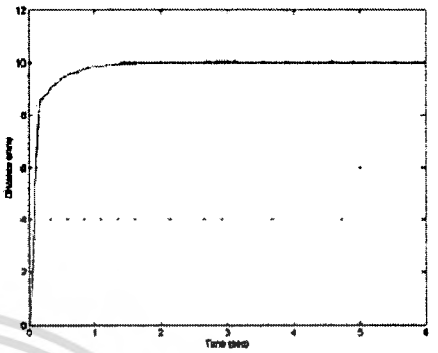

Fig. 9. Experimental result of a 10mm step response for 1kg load mass.

7. Conclusion

The position control of ultrasonic linear motor using PDFF controller designed by CDM has been proposed. It is seen that the step responses of the control system designed by CDM have no overshoot. Furthermore, the effect of disturbance is small and can be rejected rapidly, and the control system is robust to the load change. Hence, it can be concluded that the position control of ultrasonic linear motor is satisfactory by CDM.

References

[1] K.K. Tan, Tong Heng Lee, and Huixing X. Zhou, "Micro-Position of Linear-Piezoelectric Motors Based on a Learning Nonlinear PID Controller," IEEE/ASME Transactions on Mechatronics, Vol. 6, No. 4, pp. 428-436, 2001.

[2] Yuji Izuno, Ryuzo Takeda, and Mutsuno Nakaoka, "New Fuzzy Reasoning-Based High-Performance Speed/Position Servo Control Schemes Incorporating Ultrasonic Motor," IEEE Transactions on Industry Applications, Vol. 28, No. 3, pp. 613-618, 1992.

[3] Tomonobu Senjyu, Hiroshi Miyazato, and Katsumi Uezato, "Quick and Precise Position Control of Ultrasonic Motors with Two Control Inputs," Power Electronics Specialists Conference, pp. 415-420, 1995.

[4] Tomonobu Senjyu, Hiroshi Miyazato, Satoru Yokoda, and Katsumi Uezato, "Position Control of Ultrasonic Motors Using Neural Network," Power Electronics Congress CIEP'96, pp. 29-34, 1996.

[5] S.Manabe, "Coefficient Diagram Method," 14th IFAC Symposium on Automatic Control in Aerospace, 1998.

[6] Wenhuo Zeng and Jun Hu, "Application of Intelligent PDF Control Algorithm to an Electrohydraulic Position Servo System," Proceedings of the 1999 IEEE/ASME International Conference on Advanced Intelligent Mechatronics, pp. 233-238, 1999.

[7] D. Isarakorn, S. Panaudomsup, T. Benjanarasuth, J. Ngamwiwit and N. Komine, "Application of CDM to PDFF Controller for Motion Control System," The 4th Asian Control Conference, Singapore 2002.

This material is reserved for educational use only, not allowed for commercial use.
Forbidden to modify the content, and cite the document when use.

Appendix D

Design of PD Control System

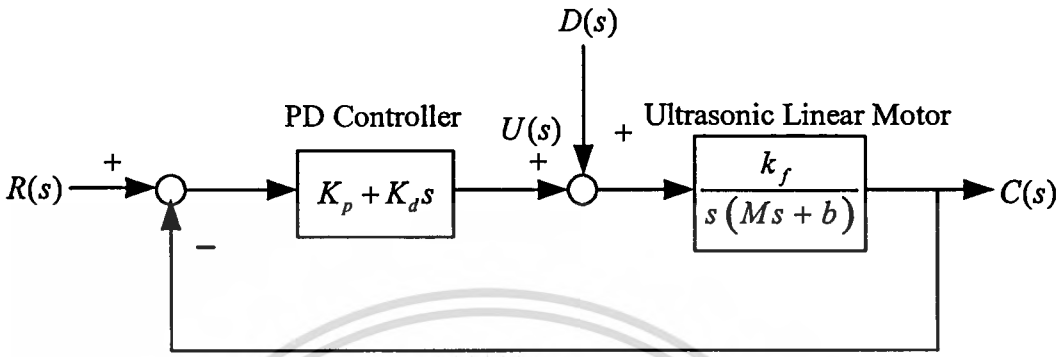

Figure D.1 PD control system structure.

The PD position control system structure shown in figure D.1 consists of a PD controller and the ultrasonic linear motor. The transfer function $G_c(s)$ of the PD controller is

$$G_c(s) = K_p + K_d s$$

where K_p and K_d are a proportional gain and a derivative gain respectively. The closed-loop transfer function of PD position control system of ultrasonic linear motor is given by

$$\frac{C(s)}{R(s)} = \frac{K_d s + K_p}{\left(M/k_f\right)s^2 + \left(K_d + b/k_f\right)s + K_p}.$$

The parameters of PD controller have been designed by pole-placement method by assigning the poles at $P_1 = -2.6$ and $P_2 = -167.4$ such that the settling time of the system is equal to the settling time of the PDFF control system. Thus, the parameters of PD controller are $K_p = 230$ and $K_d = 2$. The simulations of the PD control system shown in figure D.1 for a 20mm step input with no load mass and its control signal are shown in figure D.2 and D.3 respectively. It is seen that the system response exhibits a rise time of 0.83 second without overshoot, and a settling time of 1.47 seconds. The steady-state error is zero.

This material is reserved for educational use only, not allowed for commercial use.
Forbidden to modify the content, and cite the document when use.

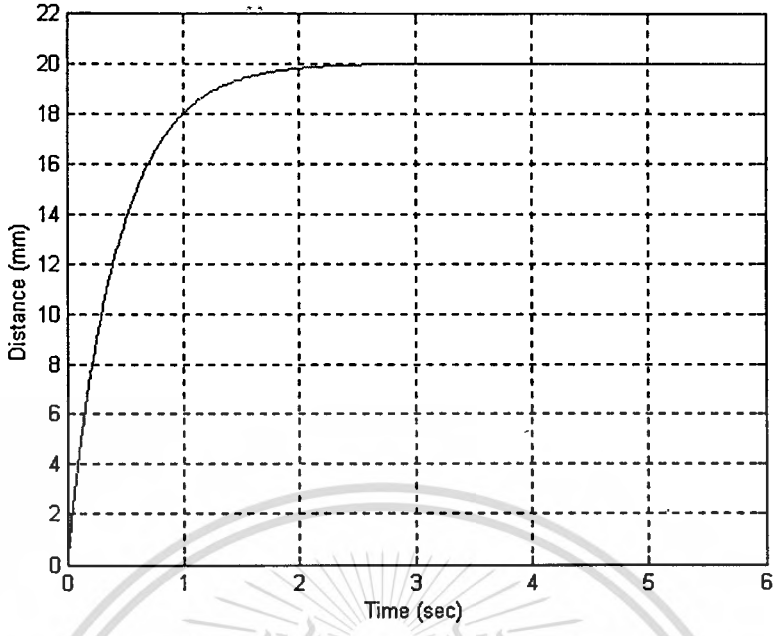

Figure D.2 Response to step input with no load mass.

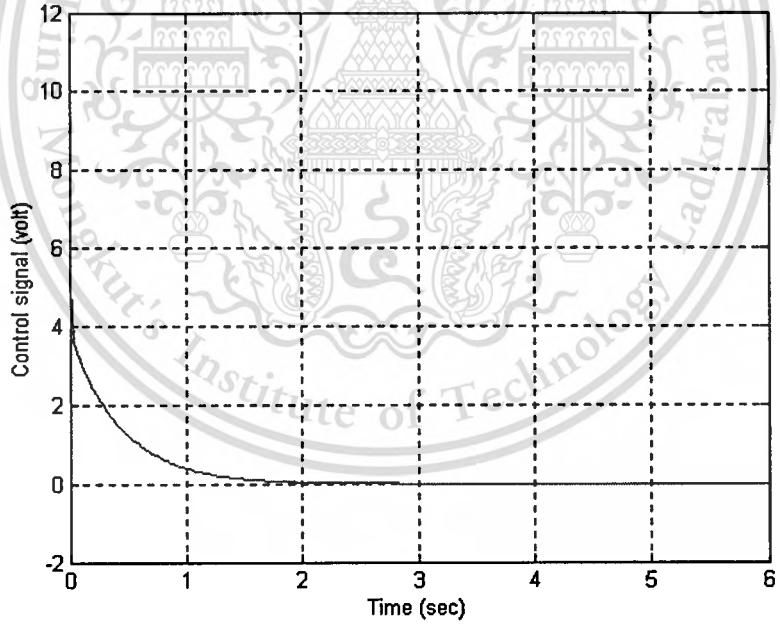

Figure D.3 Control signal.

The disturbance rejection capability has been also examined by applying a step disturbance equivalent to 1N to the system of figure D.1 at 6 seconds, while PD control system is controlling the position at 20mm. The response and the control signal are shown in figures D.4 and D.5 respectively.

This material is reserved for educational use only, not allowed for commercial use.
Forbidden to modify the content, and cite the document when use.

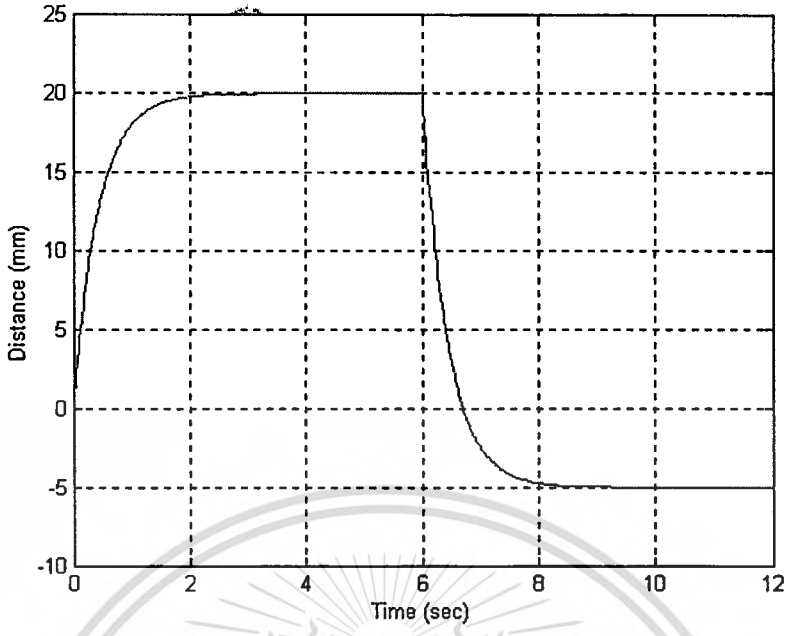

Figure D.4 Response to step input and step disturbance.

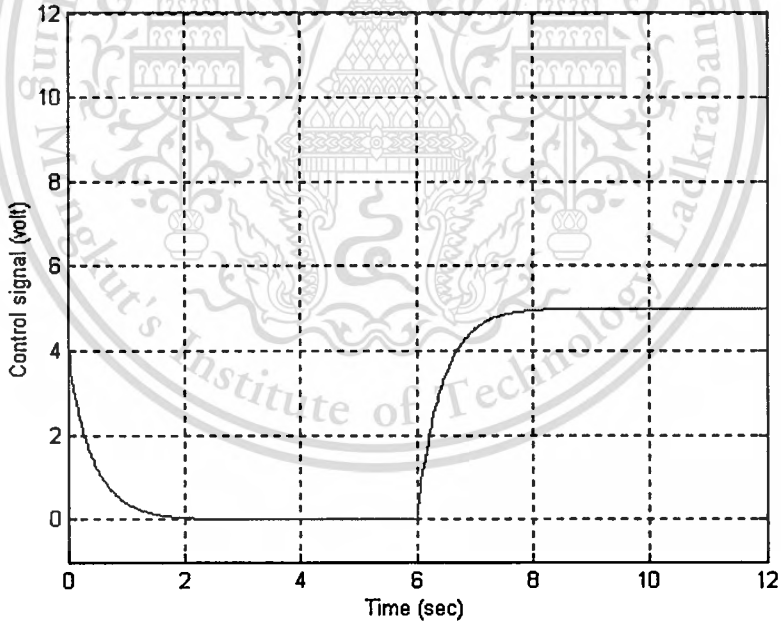

Figure D.5 Control signal.

It is seen that the steady-state error occurs by disturbance. Therefore, the PD position control system lacks of the disturbance rejection capability.

This material is reserved for educational use only, not allowed for commercial use.
Forbidden to modify the content, and cite the document when use.

Appendix E

Specifications of Piezoelectric Motor and Driver

E.1 Performance Characteristics of Piezoelectric Motor Model PDM130

Motor Speed (unloaded)	0-200 mm/sec.
Motor Speed (100g load)	0-100 mm/sec.
Driving Force	2.5 N Nominal
Operating Frequency	128-132 kHz
Time Required to Achieve Constant Speed	<8 msec.
Time Required to Achieve Complete Stop	<4 msec.
Dynamic Resolution	<1.0 micron
Power Supply	500 Vpp at a frequency corresponding to the motor resonant frequency
Motor weight	8.7 grams

E.2 Performance Characteristics of Driver Model PDA130

Operating Frequency	Range from 127.5 kHz to 133.5 kHz
Operating Temperature	50˚F (10˚C) to 122˚F (50˚C)
Input Power	+24 VDC, 250 mA Regulated Switching Supply
Control Input	-10 to +10 VDC
Output	500 40 Vpp (Waveform shall be sinusoidal with THD<2.0%)

This material is reserved for educational use only, not allowed for commercial use.
Forbidden to modify the content, and cite the document when use.

Author Biography

The author, Don Isarakorn was born in Bangkok, Thailand, on December 4, 1977. He received his B.Eng degree in Electronics Engineering in 2000 from King Mongkut's Institute of Technology Ladkrabang (KMITL). In 1999, he was accepted as an exchange student in the "Japanese University Studies in Science & Technology (JUSST)" at the National University of Electro-Communications, Tokyo, Japan for one year. In consequent year, he enrolled in the Control Engineering Department, KMITL, as a graduate student and become a member of the Control and Mechatronics Laboratory, Research Center for Communications and Information Technology (ReCCIT) to work toward his M.Eng degree. At the same year, he was supported by the Asia/Pacific Culture Center for UNESCO (ACCU) to participate in the "Technical Education Based on Micromachine Technology and Cultural Interchange Between Young Engineers" program at the Kagawa University, Japan. At that time, he developed four types of micro robots for the International Micro Robot Joint Contest authorized by Robofesta 2001, and gained three awards from them.

His main research interests include modeling, analysis and design of micromechatronics system as well as control theory.

This material is reserved for educational use only, not allowed for commercial use.
Forbidden to modify the content, and cite the document when use.